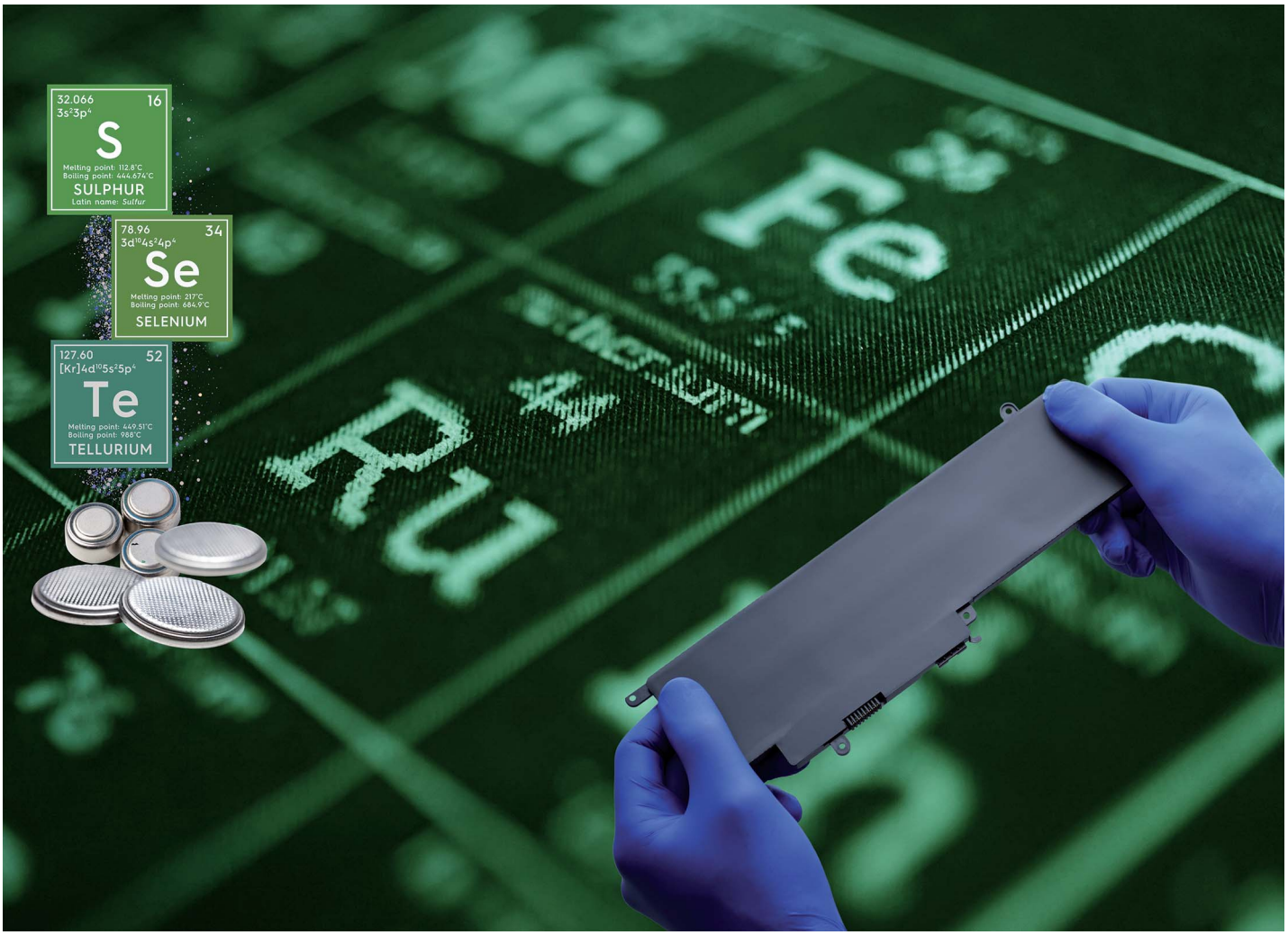


**Showcasing research from Dr. Soubantika Palchoudhury's laboratory, Chemical and Materials Engineering, University of Dayton, USA.**

Transition metal chalcogenides for next-generation energy storage

This work highlights the major breakthrough in research at the rich interface of nanochemistry for new transition metal chalcogenides and next-generation energy storage. The tunable electronic properties of chalcogenide nanocrystals galvanize new advances in alternative electrode materials for energy storage devices. Therefore, this work showcases the progress of chalcogenide nanostructures and layered mesostructure-based electrodes in lithium-ion, sodium-ion, and potassium-ion batteries and flexible supercapacitors. Cover image created by Dr. Soubantika Palchoudhury *via* Canva.com.

## As featured in:

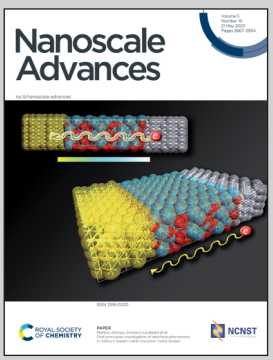


See Soubantika Palchoudhury, Arunava Gupta *et al.*, *Nanoscale Adv.*, 2023, **5**, 2724.

ROYAL SOCIETY OF CHEMISTRY

rsc.li/nanoscale-advances

Registered charity number: 207890

Nanoscale Advances

ROYAL SOCIETY OF CHEMISTRY

REVIEW

View Article Online
View Journal | View Issue

Open Access Article. Published on 24 Nyenyenyani 2023. Downloaded on 2024-08-06 15:29:40.
This article is licensed under a Creative Commons Attribution-NonCommercial 3.0 Unported Licence.

Check for updates

Cite this: *Nanoscale Adv.*, 2023, **5**, 2724

# Transition metal chalcogenides for next-generation energy storage

Soubantika Palchoudhury, *[a] Karthik Ramasamy,[b] Jinchen Han,[a] Peng Chen[a] and Arunava Gupta *[c]

Transition-metal chalcogenide nanostructures provide a unique material platform to engineer next-generation energy storage devices such as lithium-ion, sodium-ion, and potassium-ion batteries and flexible supercapacitors. The transition-metal chalcogenide nanocrystals and thin films have enhanced electroactive sites for redox reactions and hierarchical flexibility of structure and electronic properties in the multinary compositions. They also consist of more earth-abundant elements. These properties make them attractive and more viable new electrode materials for energy storage devices compared to the traditional materials. This review highlights the recent advances in chalcogenide-based electrodes for batteries and flexible supercapacitors. The viability and structure–property relation of these materials are explored. The use of various chalcogenide nanocrystals supported on carbonaceous substrates, two-dimensional transition metal chalcogenides, and novel MXene-based chalcogenide heterostructures as electrode materials to improve the electrochemical performance of lithium-ion batteries is discussed. The sodium-ion and potassium-ion batteries offer a more viable alternative to lithium-ion technology as they consist of readily available source materials. Application of various transition metal chalcogenides such as $MoS_2$, $MoSe_2$, $VS_2$, and $SnS_x$, composite materials, and heterojunction bimetallic nanosheets composed of multi-metals as electrodes to enhance the long-term cycling stability, rate capability, and

Received 23rd December 2022
Accepted 23rd February 2023

DOI: 10.1039/d2na00944g

rsc.li/nanoscale-advances

[a]*Chemical and Materials Engineering, University of Dayton, OH, USA. E-mail: spalchoudhury1@udayton.edu*
[b]*UbiQD Inc., Los Alamos, NM, USA*
[c]*Department of Chemistry and Biochemistry, The University of Alabama, AL, USA. E-mail: arunava.gupta@ua.edu*

*Soubantika Palchoudhury received her B.Tech in chemical engineering from the National Institute of Technology, Durgapur, India. She continued her graduate studies in chemical engineering and inorganic nanochemistry at The University of Alabama (UA), where she earned her M.S. and Ph.D. in 2012. She received postdoctoral training at Yale, the University of South Carolina, and the UA. She joined the University of Dayton (UD) in 2021, where she is now an Assistant Professor in Chemical Engineering. She served as a faculty member at the University of Tennessee Chattanooga prior to her appointment at the UD. Her group focuses on developing new materials for photonic and photovoltaic devices, drug delivery, and environmental applications using methods at the interface of nanochemistry, biomimetics, and material characterization.*

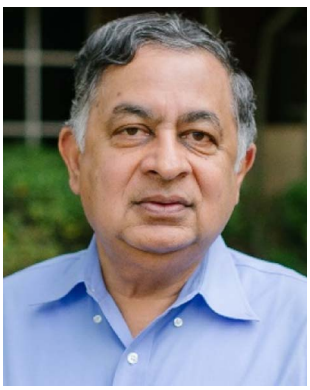

*Arunava Gupta is a distinguished university research professor at the University of Alabama (UA) with a joint appointment in the Departments of Chemistry and Chemical Engineering. Gupta received his undergraduate degree from the Indian Institute of Technology, Kanpur, and Ph.D. degree in chemical physics from Stanford University. Prior to joining the UA's faculty in 2004, he worked as a research staff member and manager at the IBM Thomas J. Watson Research Center in New York. Gupta's expertise is in investigating thin films and nanostructured materials for use in information technology and energy applications.*


© 2023 The Author(s). Published by the Royal Society of Chemistry

structural strength to counteract the large volume expansion during the ion intercalation/deintercalation processes is highlighted. The promising performances of layered chalcogenides and various chalcogenide nanowire compositions as electrodes for flexible supercapacitors are also discussed in detail. The review also details the progress made in new chalcogenide nanostructures and layered mesostructures for energy storage applications.

Open Access Article. Published on 24 Nyenyenyani 2023. Downloaded on 2024-08-06 15:29:40.
This article is licensed under a Creative Commons Attribution-NonCommercial 3.0 Unported Licence.

## 1. Introduction

With increasing energy consumption and the gradual depletion and carbon emission of finite nonrenewable energy sources, energy generation and storage from sustainable sources have become key for several modern technologies.[1–4] Modern portable and wearable electronics such as laptops, cell phones, and several health monitoring devices are made possible by electrochemical energy storage technologies including batteries and supercapacitors.[5–7] In a supercapacitor, the electrical energy is stored at the electrolyte–electrolyte interface.[8] One of the major advantages of a supercapacitor is its high specific energy. They also exhibit promising specific power. Batteries, on the other hand, use electrochemical reactions to store energy and are characterized by exceptional energy density. However, they are limited by low power densities.[9,10]

One of the most effective pathways to realize revolutionary electrochemical energy storage, beyond the scope of existing technologies and to further enhance the electrochemical performance of existing devices is through new electrode materials.[11–14] Chalcogenides constitute a promising class of novel electrode materials for both batteries and supercapacitors (Fig. 1).[15–18] Chalcogenides are compounds which contain one or more chalcogen anions such as oxygen, sulfur, selenium, and tellurium. However, oxides typically show properties that are distinct from those of other chalcogenides and are treated as a separate class of materials. Various binary and ternary compositions of chalcogenides have been reported in the literature.[19–23] Binary chalcogenide compositions are most stable and are easier to synthesize. Fewer reports of quaternary and multinary chalcogenides are available as they require higher levels of control on the synthetic parameters. However, these multinary chalcogenide compositions allow higher levels of flexibility in electrochemical properties due to their hierarchical structure.[24,25]

This review highlights the key role of various chalcogenide-based materials in catalyzing new advances in electrochemical energy storage. Application of chalcogenide nanocrystals and novel hybrid chalcogenide nanoarchitectures for lithium-ion, sodium-ion, and potassium-ion batteries and flexible supercapacitor technologies is discussed. The role of emerging chalcogenide-based electrodes in addressing the existing limitations of these energy storage technologies is highlighted from a materials perspective. The review concludes with a perspective capturing new insights into the fundamental charge transport mechanisms in novel chalcogenide electrodes and the emerging new technologies such as hybrid devices for realizing the full potential of electrochemical energy storage. Industrial

*Karthik Ramasamy is the Vice President of Materials at UbiQD Inc., where he leads research and development and manufacturing of quantum dots and nanocomposites. He received his PhD in chemistry from the University of Manchester, UK. He is a fellow of the Royal Society of Chemistry (FRSC) and an associate editor of Frontiers in Nanotechnology. He has authored/co-authored more than 65 publications and written 8 book chapters and spoken at more than 50 international meetings. He has 6 granted, published and pending patents. He can be reached at karthik@ubiqd.com.*

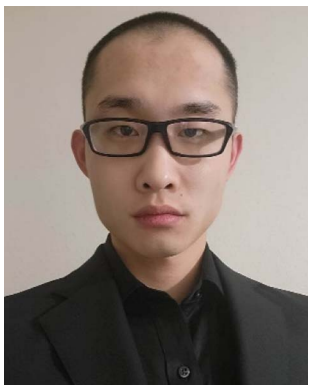

*Jinchen Han is a Ph.D. student in the materials engineering program at the University of Dayton. He earned his M.S. in materials engineering from the University of Dayton in 2021. He graduated from Shenyang Ligong University, China in 2018 with a B.S. in materials engineering and a focus on inorganic non-metallic materials.*

*Peng Chen is a recent graduate from the M.S. Chemical Engineering program at the University of Dayton. His expertise is in functionalized nanoparticles, energy materials, and materials characterization. He is currently pursuing his Ph.D. in chemical engineering at North Carolina State University.*

Open Access Article. Published on 24 Nyenyenyani 2023. Downloaded on 2024-08-06 15:29:40.
This article is licensed under a Creative Commons Attribution-NonCommercial 3.0 Unported Licence.

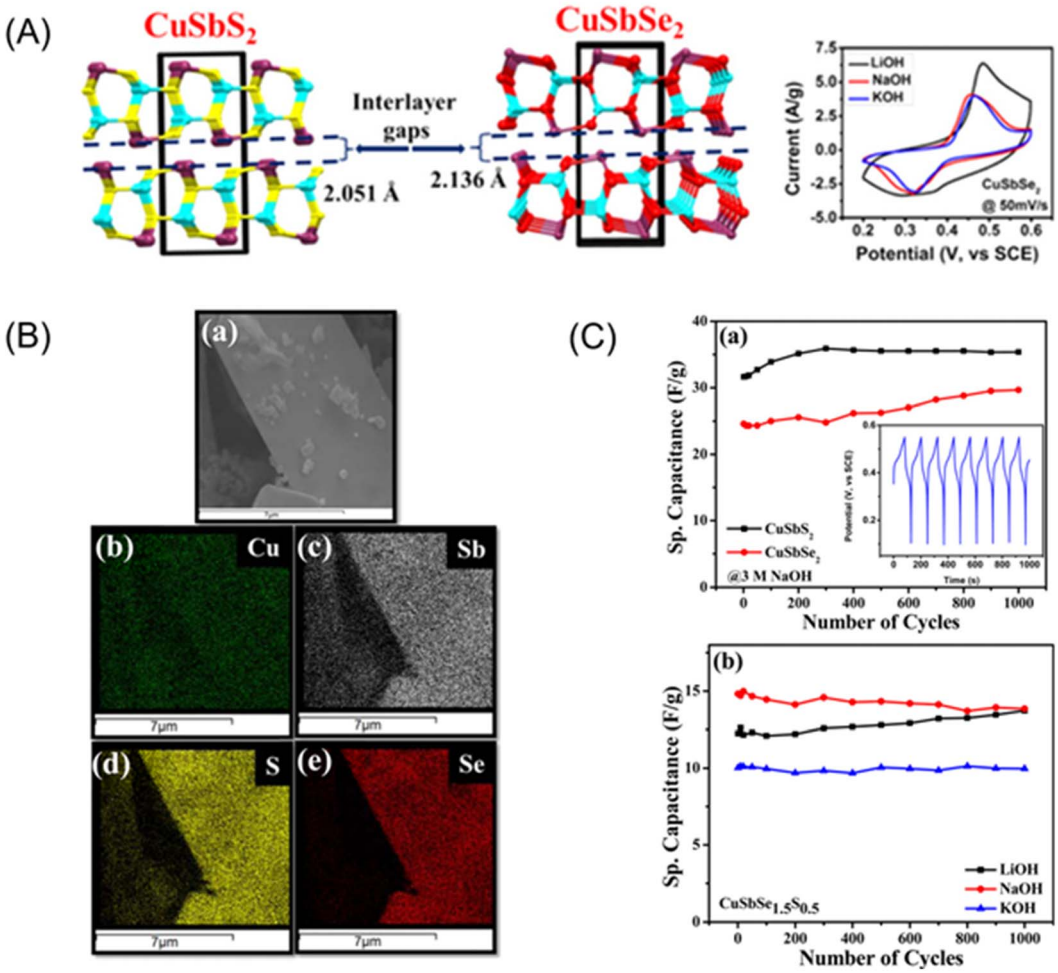


Fig. 1 Layered $CuSbSe_xS_{2-x}$, $x = 1$ mesocrystals as electrode materials for supercapacitors. (A) Schematic of the effect of interlayer spacing on the electrochemical properties of these new materials. (B) SEM-EDX mapping images of $CuSbSe_xS_{2-x}$, $x = 1$ mesocrystals showing uniform distribution of Cu, Sb, S and Se, and (C) specific capacitance and cycling performance of the new chalcogenides. (a) Cycling performance of the $CuSbS_2$ and $CuSbSe_2$ electrodes at a constant current of 0.5 mA using NaOH electrolyte. The inset shows the first few cycles of the charge–discharge curves. (b) Cyclic performance of $CuSbSe_{1.5}S_{0.5}$ using different electrolytes. Reproduced with permission from Ramasamy *et al.*, *Chem. Mater.*, 2015, **27**, 379.[28]

sectors such as electric motor vehicles are some of the major worldwide users of battery technology. Recently, there has been a growing interest to partially replace the existing lithium-ion technology with more sustainable battery technologies consisting of raw materials from widely abundant sources *e.g.*, the sodium-ion battery. The Na-ion technology is also more convenient for consumers as it minimizes safety risks and costs related to shipping and transport of the battery when compared to the Li-ion batteries. Therefore, companies such as Faradion in UK, HiNa in China, Natron Energy in USA, and Tiamat and Altris AB in Europe have focused on the development and scalable production of Na-ion batteries.[26] However, suitable anode materials like transition metal dichalcogenides with large interlayer spacings are being explored to account for the large volume expansion of the Na-ion intercalation–deintercalation process and to increase the performance efficiency of the Na-ion batteries for large-scale applications. Recently, Pang *et al.* reported another highly sustainable rechargeable battery technology consisting of aluminum, the most earth-abundant element, as the negative electrode and Se or S as the positive electrode.[27] The large-scale application potential of this energy storage technology is huge as all the raw materials are readily available, making the cost of this battery 12–16% that of the existing lithium-ion cells.

## 2. Lithium-ion batteries

Batteries are one of the key resources for electrochemical energy storage today. Among them, the lithium-ion batteries (LIBs) are most widely used worldwide since their first commercial introduction by SONY Corporation.[29] They offer a facile and rechargeable platform for powering major electronic devices used in our daily life including cell phones, laptops, iPads, wearable and portable electronics, modern electric vehicles, and storage devices for clean energy generated from renewable sources such as solar and wind.[29,30] The cathode in LIBs typically


© 2023 The Author(s). Published by the Royal Society of Chemistry

Open Access Article. Published on 24 Nyenyenyani 2023. Downloaded on 2024-08-06 15:29:40.
This article is licensed under a Creative Commons Attribution-NonCommercial 3.0 Unported Licence.

consists of a Li-intercalation compound like $LiCoO_2$ or $LiFePO_4$ while graphite serves as the traditional anode material for LIBs. The Li ions undergo intercalation and de-intercalation within the layers of the graphite anode during the discharge/charge cycle forming graphite intercalation compounds. The first Li-ion battery, developed by Yoshino used a carbon anode and $LiCoO_2$ cathode with the following electrochemical reaction:[31]

Anode:

$$C + xe^- + xLi^+ = Li_xC$$

Cathode:

$$LiCoO_2 - xe^- - xLi^+ = Li_{1-x}CoO_2$$

However, the low specific capacity of the graphite anode poses a limitation in terms of achieving the increasing demand for high energy density LIBs. New battery strategies are required to satisfy the energy density needed for realizing affordable and sustainable energy storage and distribution. Therefore, there is a continuous scientific search for suitable active anode materials with enhanced specific capacities for next-generation LIB technologies.[32] To this end, layered materials consisting of transition-metal dichalcogenides (TMDs) are promising candidates as they exhibit high specific capacities and enhanced charge/discharge capabilities.

### 2.1 Transition-metal chalcogenides for anodes

Germanium, being a homologue of carbon is an attractive alternative as an anode material for LIBs as it has a higher capacity and conductivity compared to carbon and facilitates faster diffusion of the Li-ions. However, the large volume changes during lithium alloying/dealloying and low cyclability limit its commercial viability. To this end, doping with chalcogenides such as a zinc chalcogenide doped amorphous Ge compound has been achieved *via* solvothermal synthesis to realize improved anode materials with high reversible capacity, stable capacity, and increased capacity retention.[33] The porous hierarchical morphology of this new material promotes increased ion conductivity and maintains the structural integrity by limiting the volume expansion during Li alloying/dealloying. Transition-metal selenides, having inherent high electrical conductivity and storage capacity, are also one of the most promising candidates as next-generation anode materials for LIBs, and various strategies have been implemented to improve the kinetics of Li-ion transport in these materials. For example, hybrid nanostructures of transition-metal selenides with multiwalled carbon nanotubes (CNTs) have been reported, as the CNTs are both chemically stable and serve as an excellent conductive matrix. CNTs decorated with $Co_{0.85}Se$ and $CuCo_2Se_4$ nanocrystals show high specific capacities, good cycling stability, and excellent reversible capacities even at increased current rates.[34] The unique morphology of this functionalized anode material facilitates faster transport for Li ions, provides increased active sites for electrochemical reaction, and provides a buffer for the large volume changes during $Li^+$ dealloying/alloying, thereby enhancing the electrochemical performance of the battery.

Two-dimensional TMDs offer another attractive platform as anode materials for LIBs as their unique layered structure is similar to that of the traditional graphite electrodes of LIBs, but their interlayer spacing and capacity are significantly larger.[35,36] The increased interspacing and higher surface area of these novel materials provide increased active sites for the storage of Li ions and hence facilitate faster transport of $Li^+$. Consequently, the TMD anodes show improved rate performance or capacity to generate high power with minimal voltage loss even at high current loads. They also exhibit increased pseudocapacitance. Both these properties of a TMD anode are attractive for next-generation LIBs.[37,38] Layered semiconductor TMDs such as $MoS_2$ and $WS_2$ have been integrated on conductive substrates like graphene to further augment their electrochemical performance for LIB anodes. For example, Wang *et al.* reported $MoS_2$ nanosheets on an exfoliated graphene substrate, where the graphene layer facilitates enhanced electron transport and provides structural stability during battery operation.[39] The morphology of the $MoS_2$ nanostructures plays a key role in the electrochemical performance of these anode materials. $MoS_2$ nanoflakes supported on n-doped carbon nanosheets have also been synthesized *via* a hydrothermal route and exhibit excellent capacity at high current densities, good cycling stability, as well as increased rate capacity. Different novel three-dimensional structures have been reported with $MoS_2$ for promising application as LIB anodes. In one such example, Chen *et al.* synthesized hierarchical tubular assembly of $MoS_2$ nanosheets that have been wired with CNTs for enhanced electrochemical performance in terms of specific capacity, rate capability, and cycling lifetime.[40,41] Novel hybrid nanoarchitectures have also been synthesized with other chalcogenides including $MoSe_2$, $VS_2$, $VSe_2$, $WS_2$, and $WSe_2$ for improved anode materials for LIBs.[36] In one such combination, $VS_2$ has been integrated with CNTs to form a LIB anode.[42] Carbon-coated $VSe_2$ nanosheets have also been reported using a solvothermal synthesis.[43] These materials exhibit excellent capacity, cycling stability, and rate performance as LIB anodes. Another hybrid aerogel nanoarchitecture composed of $WS_2$ nanosheets on a CNT–rGO substrate has been synthesized *via* a solvothermal approach and exhibits high specific capacity and attractive electrochemical properties as a LIB anode material.[44]

Novel heterostructures of layered two-dimensional TMDs offer the advantages of 2D materials while minimizing their limitations, which makes them promising materials for LIB anodes. These materials are synthesized *via* stacking various two-dimensional TMDs and provide higher levels of flexibility in terms of realizing high performance anodes. For example, $MoS_2$-on-MXene hetero-architectures have been reported using an *in situ* sulfidation of $Mo_2TiC_2T_x$ MXene, where the unique MXene component adds excellent conductivity and mechanical support to the heterostructure.[45] Based on first principles investigations, the high conductivity of the MXene substrate makes the heterostructure metallic although $MoS_2$ is a semiconductor. The novel $MoS_2$-on-MXene heterostructure

Open Access Article. Published on 24 Nyenyenyani 2023. Downloaded on 2024-08-06 15:29:40.
This article is licensed under a Creative Commons Attribution-NonCommercial 3.0 Unported Licence.

promotes strong Li adsorption on the two-dimensional surface and thereby exhibits excellent specific capacity, cycling stability, and rate capability. Heterostructures of intrinsically metallic TMDs like $VS_2$ have also been explored as attractive anode materials for LIBs. The advantages of each component can be integrated in these structures for an enhanced electrochemical performance. For example, the limiting stability of $VS_2$ due to Peierls distortion can be overcome through good cycling stability of the other components in the $TiO_2$-B@$VS_2$ heterostructured nanowires, while utilizing the high capacity and conductivity of the $VS_2$ chalcogenides.[46] These nanostructures exhibit an impressive reversible capacity of 365.4 mA h $g^{-1}$ after 500 cycles at 335 mA $g^{-1}$ (1C) and rate capacity (171.2 mA h $g^{-1}$ @ 10C rate).

Recently, metal–organic frameworks including MIL-96-Al, a chalcogenide-based metal–organic framework has been found to be promising electrodes for Li-based battery technologies.[47,48] It has been observed that the smaller sizes and the hexagonal bipyramidal crystal phase of this electrode material significantly improves the cycling performance of the battery by suppressing the shuttle effects. Three-dimensional ordered macroporous materials have also emerged as new and promising active materials for electrochemical energy storage as compared to the one-dimensional and 2D materials because the efficiency of light absorption, dissociation of photoinduced charge pairs, and the surface electron transfer efficiency are all enhanced within the three-dimensional structures.[49] Hollow structures can be used to tune the mass and charge transfer and have also been promising materials for energy storage.[50]

### 2.2 Li ion cathodes

TMDs have also served as promising cathode materials for LIBs.[51] For example, a novel 2D/2D heterostructure-based cathode material has been synthesized with $TiS_2$-decorated $VS_2$ flakes deposited on carbon nanotubes *via* chemical vapor deposition (CVD).[52] A thin layer of $TiS_2$ coating (thickness $\sim$ 2.5 nm) on the $VS_2$ platelets has been achieved using the atomic layer deposition (ALD) approach in this new cathode material. It protects the $VS_2$ core during the lithiation/delithiation process, which facilitates significant improvement in stability, specific capacity, and rate capacity of the electrode. Therefore, the electrochemical performance of LIBs can be enhanced through 2D heterostructure cathode materials as the capacity retention of $VS_2$ electrodes is 40% that of the novel $TiS_2$/$VS_2$ architectures.[52,53] To this end, Fang *et al.* reported a hierarchical layered structure of $VS_2$ chalcogenides on graphene nanosheets *via* a one-step hydrothermal synthesis as an effective cathode material for LIBs. The layered architecture of the electrode promotes effective transport of the Li-ions, thereby enhancing the stability and discharge capacity of the electrode as compared to the pristine $VS_2$ electrodes.[54] Table 1 shows a comparative summary of various lithium ion battery materials reported so far.

LIBs have been the dominant rechargeable battery technology over the last few decades as they exhibit high energy densities along with high power and acceptable cyclability. However, there is a continuous thrust to further improve the energy densities of LIBs and to minimize the safety risks in transport.[76] The anode material consisted of metallic Li in the first LIBs, but was subsequently replaced with graphite-based substrates due to the safety risks of metallic Li. However, the replacement also compromised the energy density of the LIBs. The first cathodes for LIBs were composed of $TiS_2$ and provided moderate energy storage capacity as it intercalated the Li ions at a low potential. A major improvement in both the potential and storage capacity of LIBs was brought about by the next phase of anode materials in the form of layered transition metal oxides. This has been accompanied by a 90% drop in the cost of LIBs over the last ten years. TMDs have emerged as promising anode materials for LIBs over the years owing to their high specific capacity, increased charge/discharge capacity, and tunable porous morphology that can promote increased ion transport and compensate the volume expansion during the Li-ion intercalation/deintercalation processes. Among them, the selenides provide higher electrical conductivity and storage capacity than the sulfide-based anodes, but they have been less explored. The two-dimensional layered TMDs and their hybrid nanoarchitectures, such as the new MXene-based materials offer further structural flexibility to achieve enhanced power and cyclability. Recently, hybrid chalcogenides like $TiS_2$/$VS_2$ architectures have also served as promising cathode materials for LIBs.

## 3. Sodium-ion batteries

Sodium-ion batteries (SIBs) have received widespread attention as an attractive alternative for LIBs, particularly for large-scale energy storage applications as sodium sources are more abundant and cost-effective as compared to lithium.[77,78] Though their operation mechanism is similar to that of LIBs, the larger size of $Na^+$ compared to $Li^+$ (1.02 Å *vs.* 0.76 Å) induces slower ion transport and electrochemical reaction kinetics. There are also considerable volume changes accompanying the charge/discharge process in SIBs. These factors limit the energy density of SIBs.[78] Additionally, the larger size and lower standard electrochemical potential of Na-ions may lead to safety issues from explosion or corrosion.[79,80] Therefore, high-capacity materials such as transition-metal chalcogenides have been explored as SIB anodes to enhance the cell density and electrochemical performance of SIBs. However, the chalcogenides inherently exhibit poor electrical conductivity and large volume expansion during the de-intercalation of Na ions.[81,82] Therefore, various novel modification strategies have been explored to further improve the electrochemical performance of the transition-metal chalcogenide anode materials including carbon doping, metal substitution, and synthesis of hybrid nanoarchitectures.[83,84] Transition to nanoscale size increases the surface area, which significantly enhances the electrode–electrolyte interaction surface and compensates for stresses from volume changes during the sodiation/desodiation process.[77,85] For example, the three-dimensional hollow nanoarchitecture form of the chalcogenides can immensely improve the electrochemical performance of the anodes as the nanoscale


© 2023 The Author(s). Published by the Royal Society of Chemistry

Open Access Article. Published on 24 Nyenyenyani 2023. Downloaded on 2024-08-06 15:29:40.
This article is licensed under a Creative Commons Attribution-NonCommercial 3.0 Unported Licence.



Table 1 Comparison of various lithium-ion battery materials that are in the developmental and commercial stages

| Active materials | Synthesis | Specific capacity | Rate | Current density | Cycling stability | Anode/cathode | Ref. |
|---|---|---|---|---|---|---|---|
| **Chalcogenides** | | | | | | | |
| $Zn_{0.81}Ge_{3.19}S_8$ | Solvothermal | 370 mA h $g^{-1}$ at 1000 mA $g^{-1}$ | | 100 mA $g^{-1}$ | 92% after 500 cycles at 1 A $g^{-1}$ | Anode | 33 |
| $Co_{0.85}Se$/CNTs and $CuCo_2Se_4$/CNT hybrids | Solvothermal | 1025 and 996 mA h $g^{-1}$ | | 100 mA $g^{-1}$ | 566 and 479 mA h $g^{-1}$ after 500 cycles | Anode | 34 |
| $WSe_2$ nanocrystals | Colloidal hot-injection | 498 mA h $g^{-1}$ | | 100 mA $g^{-1}$ | 83.28% retention | Anode | 36 |
| $MoS_2$ nanoplates | Solvothermal | 912 mA h $g^{-1}$ at 1C (1C = 1.06 A $g^{-1}$) | 658 mA h $g^{-1}$ at 30C; 554 mA h $g^{-1}$ at 50C | 50 mA $g^{-1}$ | 900 mA h $g^{-1}$ at 10C after 50 cycles | Anode | 55 |
| $Fe_3O_4/MoS_2$ composites | Hydrothermal | 1079 mA h $g^{-1}$ at 100 mA $g^{-1}$ | 569 at 4 A $g^{-1}$; 224 at 10 A $g^{-1}$ | 10 000 mA $g^{-1}$ | 1033 mA h $g^{-1}$ at 2 A $g^{-1}$ after 500 cycles | Anode | 56 |
| $WS_2$/N-doped graphene | Hydrothermal | 905 mA h $g^{-1}$ at 100 mA $g^{-1}$ | 700 mA h $g^{-1}$ at 5 A $g^{-1}$ | 100 mA $g^{-1}$ to 5000 mA $g^{-1}$ | 80% capacity retention; 905 mA h $g^{-1}$ at 100 mA $g^{-1}$ after 100 cycles | Anode | 57 |
| $MoS_x$/MWCNTs | Solvothermal | 1549 mA h $g^{-1}$ at 0.05 A $g^{-1}$ | ~200 mA h $g^{-1}$ at 2 A $g^{-1}$ | 50 mA $g^{-1}$ | 60 mA h $g^{-1}$ at 0.05 A $g^{-1}$ | Anode | 58 |
| **Oxides and other 2D materials** | | | | | | | |
| Graphene capsules | Controlled peeling of multiwalled graphitic capsules and annealing | 1373 mA h $g^{-1}$ at 0.5 A $g^{-1}$ | 750 mA h $g^{-1}$ at 8 A $g^{-1}$; 447 mA h $g^{-1}$ at 20 A $g^{-1}$ | 20 A $g^{-1}$ | 1373 mA h $g^{-1}$ at 0.5 A $g^{-1}$ after 200 cycles | Anode | 59 |
| B-doped graphene nanosheets | Chemical exfoliation and thermal reduction | 1549 mA h $g^{-1}$ at 50 mA $g^{-1}$ | 380 mA h $g^{-1}$ at 5 A $g^{-1}$; 235 mA h $g^{-1}$ at 25 A $g^{-1}$ | 50 mA $g^{-1}$ | 1227 mA h $g^{-1}$ at 50 mA $g^{-1}$ after 30 cycles | Anode | 60 |
| $ZnMn_2O_4$/graphene composites | Modified Hummers method | 730 mA h $g^{-1}$ at 500 mA $g^{-1}$ | 568 mA h $g^{-1}$ at 3.2 A $g^{-1}$ | 500 mA $g^{-1}$ | 800 mA h $g^{-1}$ at 500 mA $g^{-1}$ for 100 cycles | Anode | 61 |
| Porous ZnO nanosheets | Chemical bath deposition and heat treatment | 750 mA h $g^{-1}$ at 50 mA $g^{-1}$ | 195 mA h $g^{-1}$ at 2 A $g^{-1}$ | 500 mA $g^{-1}$ | 400 mA h $g^{-1}$ at 500 mA $g^{-1}$ after 100 cycles | Anode | 62 |
| $TiO_2$ nanocrystals/rGO sheets | Sol–gel synthesis; modified Hummers method | 189 mA h $g^{-1}$ at 0.1 A $g^{-1}$ | 94 mA h $g^{-1}$ at 10 A $g^{-1}$ | 10 A $g^{-1}$ | 189 mA h $g^{-1}$ at 0.1 A $g^{-1}$ after 100 cycles | Anode | 63 |
| $Li_4Ti_5O_{12}$ nanosheet arrays | Hydrothermal | 163 mA h $g^{-1}$ at 20C (1C = 175 mA $g^{-1}$) | 163 mA h $g^{-1}$ at 20C; 78 mA h $g^{-1}$ at 200C | 20–200C | 124 mA h $g^{-1}$ at 50C after 3000 cycles | Anode | 64 |
| **Cathode materials** | | | | | | | |
| $LiFePO_4$ nanosheets | Solvothermal | 151 mA h $g^{-1}$ at 0.5C (1C = 170 mA $g^{-1}$) | 120 mA h $g^{-1}$ at 5C; 55 mA h $g^{-1}$ at 30C | 1–30C | 90 mA h $g^{-1}$ at 10C after 1000 cycles | Cathode | 65 |
| $LiFePO_4$/C nanosheets | Liquid-phase exfoliation and solvothermal lithiation | 164 mA h $g^{-1}$ at 0.2C | 70 mA h $g^{-1}$ at 80C | 80C | 163 mA h $g^{-1}$ at 0.2C after 50 cycles | Cathode | 66 |
| $LiMnPO_4$/C nanosheets | Liquid-phase exfoliation and solvothermal lithiation | 157 mA h $g^{-1}$ at 0.2C | 40 mA h $g^{-1}$ at 30C | 30C | 147 mA h $g^{-1}$ at 0.2C after 50 cycles | Cathode | 66 |
| $LiCoPO_4$/C nanosheets | Liquid-phase exfoliation and solvothermal lithiation | 153 mA h $g^{-1}$ at 0.2C | 53 mA h $g^{-1}$ at 20C | 20C | 136 mA h $g^{-1}$ at 0.2C after 50 cycles | Cathode | 66 |
| **MXene-based materials** | | | | | | | |
| $Mo_2TiC_2$ (MXene) | Exfoliation | 269 mA h $g^{-1}$ at C/10 | 176 mA h $g^{-1}$ at 1C | 1C | 260 mA h $g^{-1}$ at C/10 after 25 cycles | Anode | 67 |
| MXene/CNT paper | Ball mill | 420 mA h $g^{-1}$ at 0.5C | 270 mA h $g^{-1}$ at 10C; 160 mA h $g^{-1}$ at 20C | 20C | 430 mA h $g^{-1}$ at 2.5C after 300 cycles | Anode | 68 |

© 2023 The Author(s). Published by the Royal Society of Chemistry

Open Access Article. Published on 24 Nyenyenyani 2023. Downloaded on 2024-08-06 15:29:40.
This article is licensed under a Creative Commons Attribution-NonCommercial 3.0 Unported Licence.

Table 1 (*Contd.*)

| Active materials | Synthesis | Specific capacity | Rate | Current density | Cycling stability | Anode/cathode | Ref. |
|---|---|---|---|---|---|---|---|
| **Materials that have been commercialized** | | | | | | | |
| $LiTiS_2$ | CVD-based template synthesis | 210 mA h $g^{-1}$ | — | 1.5 mA $cm^{-2}$ | — | Cathode | 69 |
| $LiCoO_2$ | Hydrothermal | 148 mA h $g^{-1}$ | 140 mA $g^{-1}$ | 1C (=140 mA $g^{-1}$) | 138.6 mA $g^{-1}$ after 20 cycles | Cathode | 70 |
| $LiNi_{0.33}Mn_{0.33}Co_{0.33}O_2$ | Co-precipitation | 160 mA h $g^{-1}$ | 190 mA $g^{-1}$ | 280 mA $g^{-1}$ | — | Cathode | 71 and 72 |
| $LiMn_2O$ | Solid-state synthesis and spray drying | 120 mA h $g^{-1}$ | 1300 mA $g^{-1}$ @ 10C (1C = 130 mA $g^{-1}$) | 130 mA $g^{-1}$ | — | Cathode | 73 |
| $LiFePO_4$ | Solid-state reaction | 165 mA h $g^{-1}$ | — | >1 mA $cm^{-2}$ | — | Cathode | 74 and 75 |

size shortens the $Na^+$ ion transmission distance while the hollow morphology counteracts the volume expansion during the de-intercalation of Na-ions.[86] Metal substitution is another key strategy that is known to enhance the rate performance of the chalcogenide anodes, as observed for the case of Co-substituted $FeS_2$.[87,88] Similarly, metal-substituted $CoS_2$@$Cu_xS$ nanostructures exhibit higher capacity (535 mA h $g^{-1}$ @ 0.1 A $g^{-1}$), discharge rate (333 mA h $g^{-1}$ @ 5 A $g^{-1}$) and cycle capacity (76% capacity retention over 300 cycles) as compared to the parent $CoS_2$ electrode (*e.g.*, 249.0 mA h $g^{-1}$ at 0.5 A $g^{-1}$ and 1000 cycles at 1 A $g^{-1}$).[78,89] Other novel hybrid nanostructures have been realized that combine a single layer of $MoSe_2$ onto the surfaces of core–shell $Fe_7Se_8$@C structures.[90] This hybrid chalcogenide anode material vastly improves the stability and retention rate of the battery.

Layered two-dimensional TMDs (*e.g.*, $VS_2$, $MoS_2$, and $CoS_2$), with their unique interlayer spacings and high theoretical storage capacity, provide an ideal platform for rapid intercalation/de-intercalation of Na ions and are attractive anode materials for SIBs.[85] For example, hierarchical 2D nanoflake ensembles of $VS_2$ facilitate improved transport of $Na^+$ and significantly improve the electrochemical performance of the battery.[91] Anode materials containing $VS_2$ chalcogenides with a flower-like morphology have also been reported and these nanostructures promote superior rate performance as well as excellent long-term cycling stability in SIBs.[92] Apart from $VS_2$, various layered $MoS_2$ and $MoSe_2$ chalcogenide nanostructures have been reported as key electrode materials for SIBs (Fig. 2).[93,94] Na-ions are stored in these materials *via* a two-step process, intercalation at higher potential and conversion in a lower potential window as follows:[95]

$$MoS_2 + xNa \rightleftharpoons Na_xMoS_2 \ (>0.4\ V,\ x < 1.5)$$

$$Na_xMoS_2 + (4 - x)Na \rightleftharpoons Mo + 2Na_2S \ (<0.4\ V)$$

The interlayer spacing of these materials plays a crucial role in improving the electrochemical performance of the battery as the capacity and rate capability of the SIB increases with the interlayer distance in $MoS_2$ nanoflake-based anodes. In addition, electrode materials consisting of hybrid nanoarchitectures of chalcogenides supported on one-dimensional substrates, such as $MoS_2$ decorated n-doped carbon ribbon and core–shell $MoSe_2$@n-doped carbon shell structures also facilitate significant improvement in the cycling stability, reverse capacity, and capacity of the battery. Sun *et al.* reported novel hierarchical nanohybrid anode materials with $MoS_2$ on a two-dimensional graphene substrate.[96] These electrodes have exhibited key enhancements in the current density, rate capability, as well as cycling stability of the SIB. In another report, graphene oxide cross-linked with hollow carbon spheres has been used as a novel 2D scaffold for $MoS_2$ nanoflakes.[97] The porous morphology of this novel electrode material offers a unique solution to counteract the volume expansion in SIBs and to promote enhanced transport of electrolytes, ions, and electrons. New SIB anode materials have also been reported with $MoS_2$ nanoflakes vertically aligned on conductive carbon paper.[98] The


© 2023 The Author(s). Published by the Royal Society of Chemistry

Open Access Article. Published on 24 Nyenyenyani 2023. Downloaded on 2024-08-06 15:29:40.
This article is licensed under a Creative Commons Attribution-NonCommercial 3.0 Unported Licence.

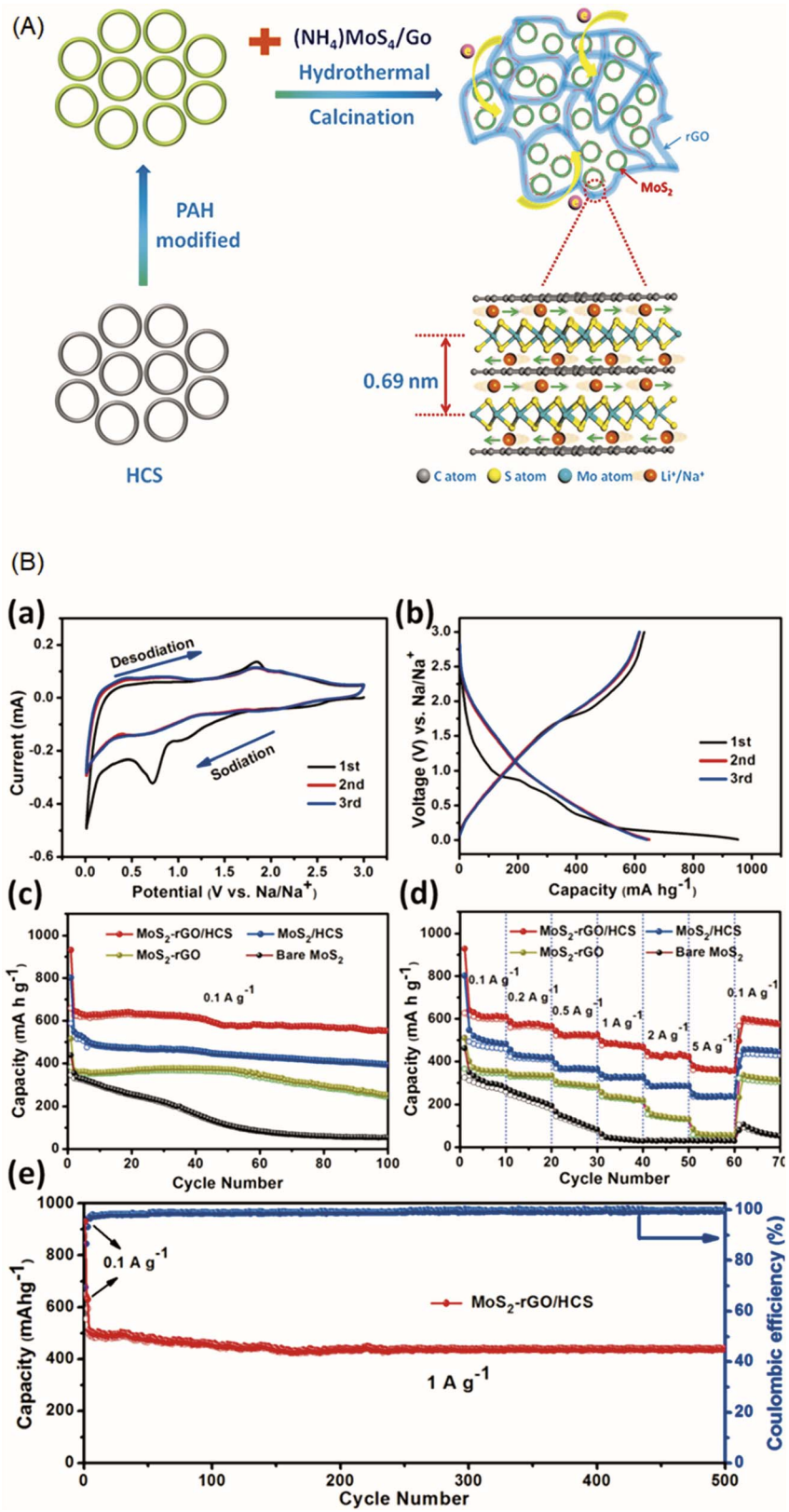


Fig. 2 Three-dimensional hybrid architecture of few layer $MoS_2$ on reduced graphene oxide (rGO) cross-linked hollow carbon spheres (HCS). (A) Schematic Illustration of the formation process of $MoS_2$–rGO/HCS and (B) electrochemical performance of the $MoS_2$–rGO/HCS for sodium storage. (a) Representative CV curves of the $MoS_2$–rGO/HCS electrode in a voltage range of 0.01 to 3.0 V and at a scan rate of 0.1 mV $s^{-1}$. (b) Charge–discharge voltage profiles of the $MoS_2$–rGO/HCS electrode at a current density of 0.1 A $g^{-1}$. (c) Cycling performance and (d) rate capability of $MoS_2$–rGO/HCS, $MoS_2$/HCS, $MoS_2$–rGO, and bare $MoS_2$. (e) Cycling performance and coulombic efficiency of $MoS_2$–rGO/HCS for 500 cycles at a current density of 1 A $g^{-1}$. Reproduced with permission from Hu *et al.*, *ACS Nano*, 2018, **12**, 1592.[97]

Open Access Article. Published on 24 Nyenyenyani 2023. Downloaded on 2024-08-06 15:29:40.
This article is licensed under a Creative Commons Attribution-NonCommercial 3.0 Unported Licence.

three-dimensional carbon fiber matrix offers increased active sites and ion/electron transfer channels to enhance the reaction kinetics of the electrochemical reactions in SIBs.

$SnS_x$-based anodes are the second most widely researched materials for SIBs due to their key advantages of eco-friendliness, high capacity, and huge natural abundance.[99,100] The large interlayer spacing of $SnS_x$ allows facile intercalation/de-intercalation of Na ions for improved reaction kinetics. The material has the capacity for storing Na ions during the conversion process as well as the intercalation/de-intercalation process through the following reaction:

$$4Sn + 15Na^+ + 15e^- \leftrightarrow Na_{15}Sn_4$$

The storage capacity of $SnS_x$ is therefore higher compared to that of the other materials, making it attractive for SIBs. Various novel strategies have been applied to $SnS_x$-based materials to further improve the limiting electrochemical properties including poor stability, high stress from volume changes, and low conductivity. Xiong *et al.* reported a hybrid nanostructure with SnS nanoparticles on a conducting n-doped graphene scaffold.[99] The graphene support minimized aggregation of the nanoparticles and greatly improved the retention rate of the SIB. In another study, a novel nanosheet morphology of $SnS_2$ has facilitated enhanced active sites for the electrochemical reactions while the unique structural features of the rGO substrate allow rapid transport of Na ions and provide structural stability to withstand changes in volume. As a result, the composite anode shows excellent charge capacity (630 mA h $g^{-1}$ at 0.2 A $g^{-1}$), rate performance (544 mA h $g^{-1}$ at 2 A $g^{-1}$), and cycling stability (500 mA h $g^{-1}$ at 1 A $g^{-1}$ for 400 cycles). Liu *et al.* synthesized a unique composite anode with $SnS_2$ nanoparticles decorated on reduced graphene oxide nanoribbons with a paper-like morphology that has induced remarkable enhancements in the discharge capacity of the battery.[101] $SnSe_x$-based electrodes, though less widely reported in the literature, have recently been synthesized *via* novel hydrothermal approaches and exhibit improved rate performance and cycling stability.[102–104] Various composite electrodes based on other transition metal chalcogenides such as $CoS_x/Se_x$, $NiS_x/Se_x$, and $WS_x/Se_x$ have also been explored as promising materials for SIBs.[44,105–115] In a recent report, novel composites of $NiSe_2$ enclosed in boron carbonitride nanotubes have been synthesized *via* a facile pyrolysis approach.[116] These anodes show excellent reversible $Na^+$ storage capacity and long-term cycling stability. In general, the reaction kinetics and decay mechanisms are similar for both S and Se-based electrode materials. Various novel carbonaceous substrates have been reported to overcome the issues of conductivity and volume changes. Se-based electrodes offer a more suitable platform for next-generation SIBs as they possess a larger interlayer spacing and intrinsic conductivity compared to sulfides.

Recently, multi-metal chalcogenides have emerged as highly promising electrode materials for SIBs as the multiple metallic centers provide enhanced adsorption capability and conductivity as well as increased active sites for the electrochemical reactions. Chen *et al.* synthesized heterojunction bimetallic sulfide nanosheets of the $SnS_2/FeS_2$/rGO composite, which have shown highly improved capacities.[117] New materials containing multiple transition metals (*e.g.*, $NiCo_2S_4$ and $Cu_2NiSnS_4$) as well as multi-phase components (*e.g.*, ZnS–$Sb_2S_3$, $NiS_2$–$CoS_2$, and $Co_9S_8$–ZnS) have been realized. In general, the electrochemical performance of the multi-metal chalcogenides significantly surpasses that of single component transition-metal chalcogenides.[118–123] However, these materials are synthetically challenging to achieve with a few reports on sulfide-based structures and limited reports on the selenides. Further insights on a compatible carbonaceous support and avenues to enhance the theoretical capacity will help make these materials viable next-generation electrodes for SIBs.

All solid-state SIBs have been another innovative alternative to LIBs and have emerged as an area of major scientific research in recent years.[124] A solid-state electrolyte is used in this battery technology that holds the advantages of being leak-free as well as having high thermal stability as compared to the traditional liquid electrolytes. A vast range of inorganic solid electrolytes for SIBs comprise various chalcogenides such as the $Na_3MS_4$ series,[125–128] the $Na_3MSe_4$ (M = P, Sb) series,[129,130] or the $Na_7P_3X_{11}$ (X = O, S, Se) series.[131] These electrolytes are appealing and cost-effective alternatives to oxides as they can be synthesized at lower temperatures. However, chalcogenide-based electrolytes can be unstable in air and can contain voids that have a detrimental impact on the materials' conductivity. Therefore, several modification strategies including doping of cations at the P site or halogen ions at the S site, forming hybrid organic–inorganic composites like polyethylene oxide-based $Na_3PS_4$, high-temperature heat treatment for crystal transformation, and ceramization and vitrification have been effectively explored to increase the stability, electrochemical performance, and mechanical properties of these next-generation solid-state chalcogenide electrolytes.[132–138]

SIBs contain source materials that are cost-effective, abundantly available on earth, and do not pose any safety concerns. Therefore, they provide an attractive and more sustainable alternative to the existing lithium-ion technology. However, the large volume expansion during the charge/discharge process and the slower ion transport due to the larger size of the Na ion limit the energy density of SIBs in comparison to that of Li-ion batteries. Therefore, transition metal chalcogenides with high specific capacities have been explored as active electrode materials for SIBs. Strategies such as carbon doping, metal substitution, formation of hybrid structures with transition metal chalcogenides, as well as using the nanoscale form of the chalcogenides have been used to enhance the electrical conductivity of these chalcogenide-based SIB electrodes. Furthermore, two-dimensional TMDs such as $MoS_2$ nanoflakes, $MoSe_2$, and $VS_2$ have been used to improve the cycling stability, rate capacity, and current density of SIBs. Various hybrid morphologies of $SnS_x$-based chalcogenides serve as promising electrode materials for SIBs owing to the higher storage capacity of Sn. Finally, all solid-state SIBs are also attractive as next-generation SIB electrodes as they are leak-free and thermally more stable compared to the existing liquid electrolytes.


© 2023 The Author(s). Published by the Royal Society of Chemistry

Open Access Article. Published on 24 Nyenyenyani 2023. Downloaded on 2024-08-06 15:29:40.
This article is licensed under a Creative Commons Attribution-NonCommercial 3.0 Unported Licence.

## 4. Potassium-ion batteries

Although LIBs have revolutionized battery technology in terms of an uninterrupted energy supply for wearable devices, electric vehicles, and stationary energy storage, the limited global reserves of lithium have been an impediment to realizing affordable technologies. To this end, SIBs and recently, potassium-ion batteries (PIBs) have been explored as alternative materials to achieve a more sustainable, affordable, and high-performance rechargeable battery technology.[139] There are a couple key theoretical advantages of PIBs as compared to the LIB and SIB technology. PIBs can ideally attain higher working voltages compared to their Li and Na counterparts as the standard redox potential of $K^+/K$ (−2.93 V *vs.* SHE) is comparable to that of $Li^+/Li$ (−3.04 V *vs.* SHE). $K^+$ is also a weaker Lewis acid and its higher diffusion rate and ionic conductivity facilitate a favorable and reversible intercalation with the graphite anode compared to the irreversible intercalation in SIBs.[140–142] A suitable anode material with superior specific capacities, cycling stability, diffusion rate, and reaction kinetics is one of the key aspects for achieving efficient and practically applicable PIB technology.

Two-dimensional metal chalcogenides (*e.g.*, $MoS_2$, $VS_2$, $SnS_2$, and $Sb_2S_3$) with low energy barriers for alkali metals and large specific capacities are highly attractive as anode materials for PIBs (Fig. 3 and 4).[139] These chalcogenide anode materials for PIBs can be primarily classified as the conversion type or conversion/alloying type based on the mechanism of potassium insertion in the anode materials.[143–146] The metal and chalcogen are electrochemically inactive for the conversion type materials while the metal atoms in the conversion/alloying anode materials have the ability to store potassium *via* alloying reactions. In the conversion-type materials (*e.g.*, $MoS_2$, $FeS_2$, ZnS, and $V_5S_8$), the chalcogen component is the primary contributor of specific capacity while the inactive metal atom serves to provide a continuously conductive platform.[91,140,147,148] Metals from group 14 and 15 constitute the active metallic component in the conversion/alloying type chalcogenide anode materials (*e.g.*, $Sb_2S_3$, $SnS_2$, and GeSe) for PIBs. The metal and chalcogen both form reversible alloys with the potassium ion, thereby

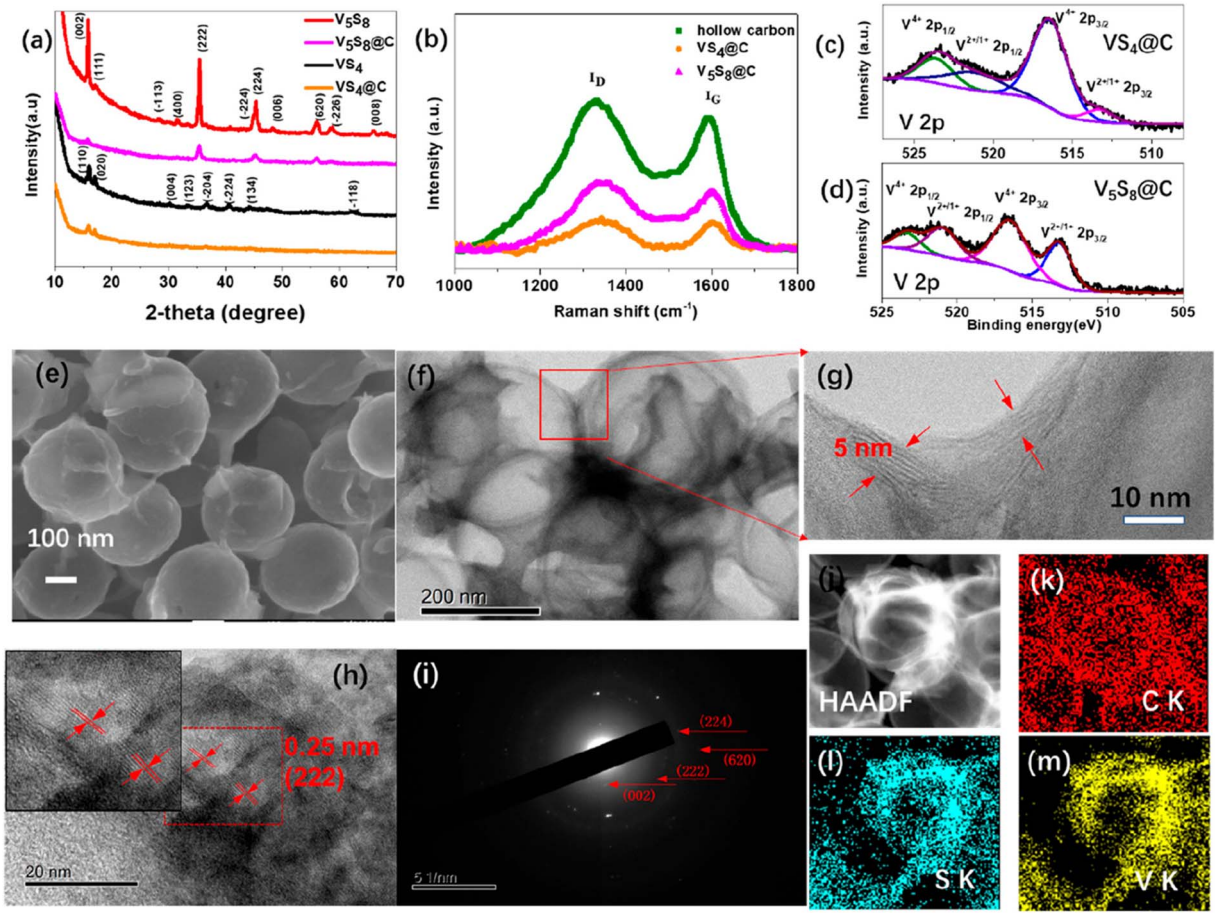


Fig. 3 Hollow-carbon-templated few-layered $V_5S_8$ nanosheets for PIBs. (a) X-ray diffraction patterns of bare $VS_4$, bare $V_5S_8$, $VS_4$@C, and $V_5S_8$@C; (b) Raman spectra of hollow carbon, $VS_4$@C, and $V_5S_8$@C; X-ray photoelectron spectroscopy of (c) $VS_4$@C: V 2p and (d) $V_5S_8$@C: V 2p; SEM image (e); TEM images (f); high-resolution TEM images (g and h); inset of (h) is the enlarged part of the red circle; selected area electron diffraction (i) of $V_5S_8$@C; STEM image (j); and elemental mapping analysis of $V_5S_8$@C: (k) C, (l) S, and (m) V elements. Reproduced with permission from Li *et al.*, *ACS Nano*, 2019, **13**, 7939.[150]

Open Access Article. Published on 24 Nyenyenyani 2023. Downloaded on 2024-08-06 15:29:40.
This article is licensed under a Creative Commons Attribution-NonCommercial 3.0 Unported Licence.

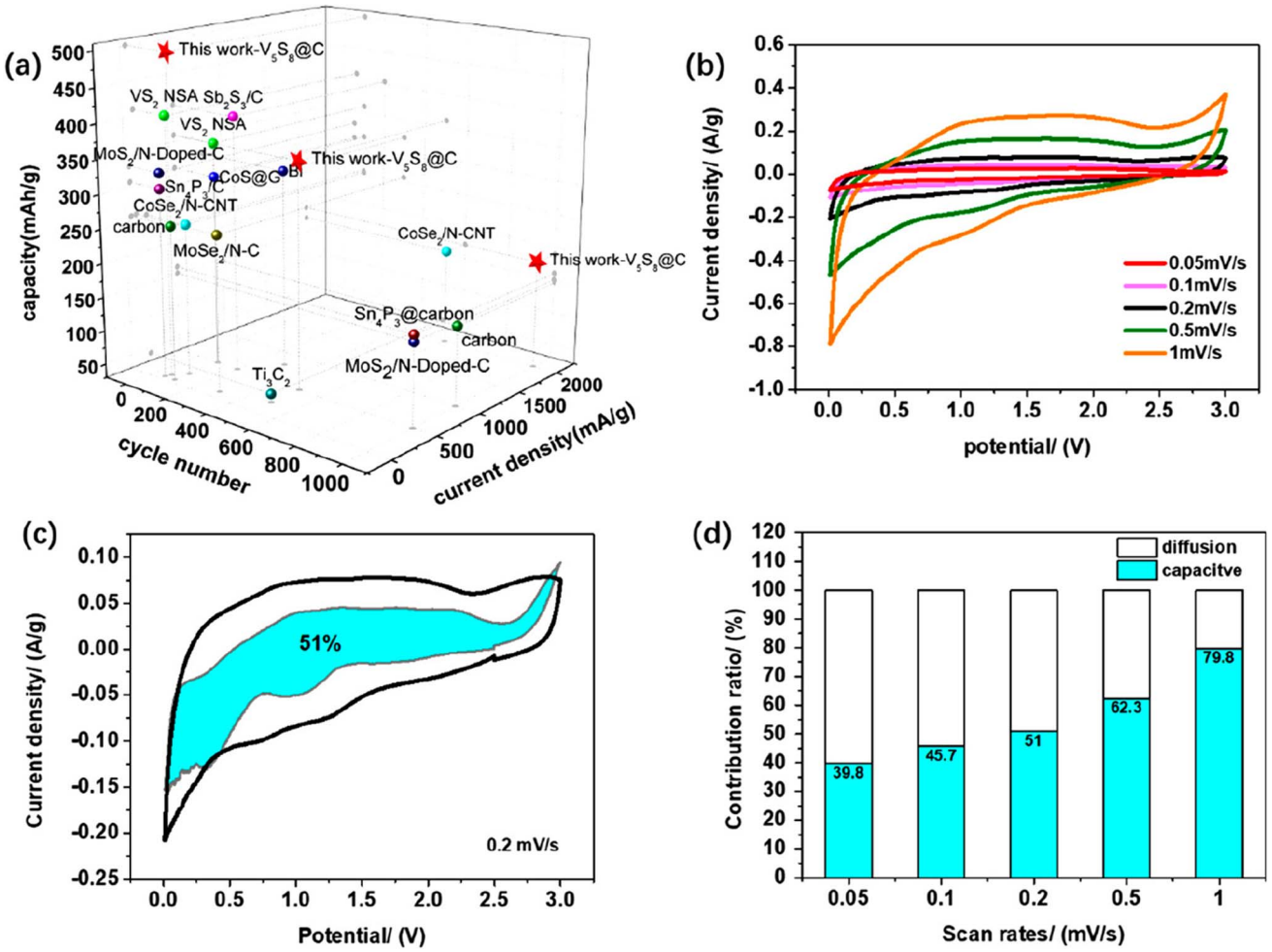


Fig. 4 (a) Comparison of the capacity and cycling capabilities of the state-of-the-art KIB anode materials with our work; (b) CV curves of $V_5S_8$@C at different scan rates from 0.05 to 1 mV $s^{-1}$; (c) CV curves of $V_5S_8$@C with separation between the total current (black line) and surface capacitive current (blue regions) at 0.2 mV $s^{-1}$; (d) capacity ratios between diffusion and capacitive contributions of $V_5S_8$@C at different scan rates from 0.05 to 1 mV $s^{-1}$. Reproduced with permission from Li *et al.*, *ACS Nano*, 2019, **13**, 7939.[150]

enhancing the capacity of this type of anode material. The detailed mechanism of potassiation/depotassiation of $MoSe_2$ anodes was first investigated by Lu *et al.* through a combination of XRD and Raman spectroscopic characterization of the materials at different phases of charge/discharge.[148] It was discovered that this electrochemical potassiation proceeds *via* a two-step process consisting of $K^+$ intercalation and conversion, with the Se chalcogen facilitating the K–Se redox reaction, similar to the reaction mechanism in Li–S batteries. Guan *et al.* reported that the potassiation of $FeS_2$ based anode materials proceeds through an initial irreversible transformation to $K_xFeS_2$, which is followed by reversible intercalation and conversion stages.[149] The charge and discharge mechanisms in another anode material, $Sb_2S_3$ were investigated using synchrotron XRD. Intercalation of $K^+$ within the $Sb_2S_3$ structure first expands the interlayer distances prior to the conversion and alloying reactions. Xia *et al.* reported the potassiation/depotassiation mechanism in $SnS_2$ materials using XRD and *in situ* TEM.[144] One of the limitations of the conversion/alloying materials is the large volume expansion associated with the potassiation process.

### 4.1 Challenges

The current state-of-the-art chalcogenide anode materials are highly attractive for potassium storage; however, some limitations still exist in the technology in terms of practical applicability.[141,151,152] For example, detrimental side reactions during the deep potassiation phase, lead to formation of potassium polychalcogenide compounds that hinder the diffusion of $K^+$ by forming a film on the metal surfaces and thereby reduce the capacity of the device.[143,150,153] Another limitation of the chalcogenide anode materials is the low structural stability caused by the large volume expansion and partially reversible phase transformations during their charge/discharge cycles. The bulk chalcogenides exhibit low electric and ionic conductivity, which detrimentally affect the diffusion of $K^+$ and electron transport mechanisms. Therefore, there is a continued scientific interest to overcome these challenges in the chalcogenide anode


© 2023 The Author(s). Published by the Royal Society of Chemistry

Open Access Article. Published on 24 Nyenyenyani 2023. Downloaded on 2024-08-06 15:29:40.
This article is licensed under a Creative Commons Attribution-NonCommercial 3.0 Unported Licence.

materials for achieving practically viable and high-performance PIB technologies.

### 4.2 Technological solutions

To this end, a few key technological strategies have been explored to improve the long-term cycling stability and capacity of chalcogenide anode materials. Wu *et al.* applied a novel approach of tuning the discharge depth during the $K^+$ intercalation in $MoS_2$ to facilitate the formation of $K_{0.4}MoS_2$ as the degradation product.[154] $K_{0.4}MoS_2$ exhibited a lower volume expansion as compared to $MoS_2$ and thereby minimized the detrimental effects on the structural integrity of the anode. Another approach by Shu *et al.* prevented the capacity loss in $TiSe_2$ materials due to irreversible depotassiation through pretreatment cycles that facilitated the formation of $K_{0.24}TiSe_2$.[155] $K_{0.24}TiSe_2$ serves as a suitable host material for $K^+$ intercalation for reversible potassium conversion reactions.

Another strategy for improving the chalcogenide anodes is *via* incorporation of carbon nanophases. The nanophase carbon provides a stable platform for minimizing the aggregation and volume expansion of the chalcogenides during the potassiation and depotassiation processes and enhances the structural integrity of the anode materials. The carbon nanophase–metal chalcogenide hybrid composites also show increased electrical conductivity as the carbon component facilitates a faster electron transfer channel for the chalcogenides. These metal chalcogenide–carbon nanophase hybrid structures can be realized by either embedding the small metal chalcogenides within the carbon matrix or by encapsulation of the chalcogenides with carbon. For example, the electrospinning approach has been effectively used for embedding graphene-coated $FeS_2$ chalcogenide nanoparticles within carbon nanofibers.[153] An improved cycling stability of PIBs has been observed with the $FeS_2$–graphene–carbon nanofiber composite anode material.[153] Electrospinning-based approaches have also proved effective for other chalcogenide nanoparticles like $VSe_{1.5}$, where the $VSe_{1.5}$ embedded carbon nanofiber composite showed stable capacity as the carbon component minimized aggregation and transport of the nanoparticles during cycling.[156] In another novel hybrid chalcogenide nanoparticle-based composite anode, CoS nanoparticles have been encapsulated at the ends of carbon nanotubes as well as on the surfaces of n-doped carbon nanofibers *via* an *in situ* CVD and electrospinning synthetic strategy.[157] This hybrid nanocomposite facilitates enhanced capacity (400 mA h $g^{-1}$) and good cycling stability (*i.e.*, 130 mA h $g^{-1}$ at 3.2 A $g^{-1}$ after 600 cycles) in PIBs owing to the efficient confinement of aggregation and migration of the chalcogenide nanoparticles. Guan *et al.* reported a unique yolk–shell structure consisting of an $FeS_2$ core with an outer carbon shell to control the volume expansion during potassiation and depotassiation.[149] The ability to accommodate volume expansion is a key advantage of the yolk–shell nanostructure as it protects the structural integrity of the anode. The confinement effect within the carbon shell also facilitates enhanced ion and electron transport in the yolk–shell nanostructures.

Ternary alloying is a novel material strategy in which a third cation or anion is used as a key tool to enhance the vacancies and realize tunable electronic and physical properties in the metal chalcogenide anode materials. For example, Guo *et al.* synthesized MoSSe nanoplates as PIB anode materials *via* a novel alloying strategy where the 1 : 1 S/Se stoichiometric ratio facilitates enhanced vacancy concentration.[158] The vacancy sites in this novel ternary material increases electron transfer and minimizes $K^+$ ion adsorption during cycling.[158] These properties of the MoSSe alloy impart enhanced reversible capacity and cycling stability to the PIB anode. Hybrid PIB anode materials constituting a layered graphene substrate containing ternary chalcogenide nanodots that are prepared *via* substitution of cations, *e.g.*, $SnSb_2Te_4$ have also shown enhanced ionic and electric conductivity.[159] A modified ball-milling approach has been used to synthesize these anodes. Wang *et al.* synthesized ternary $Ta_2NiSe_5$ nanosheets *via* a novel ion-intercalation based exfoliation method as anode materials for PIBs.[160] These ternary chalcogenides exhibit a large capacity as well as stable cyclability, which is attractive for potassium storage owing to their multiple Se sites.

Finally, synthesizing the chalcogenide materials at the nanoscale can be used as a niche strategy to address the limited ionic and electrical conductivities of the bulk phases.[161,162] A higher flexibility in obtaining a tunable structure–property relationship can be achieved at the nanoscale owing to the available surface area. The nanoparticles offer a shorter diffusion pathway, improved electron transport, and accommodation for the volume expansion during the potassiation/depotassiation cycles, which are key to maintaining the structural integrity of the anode and enhancing the potassiation/depotassiation length. Consequently, these metal chalcogenide nanostructures can serve as a next-generation platform for the anode material of PIBs in terms of enhanced capacity and cycling stability. A few key synthetic approaches used for chalcogenide nanocrystals include chemical vapor deposition, solution-based processes, hydrothermal, calcination, and hard/soft templating.[139,140,147,156,163] For example, Wang *et al.* reported a novel solvothermal synthesis of PIB anode materials containing octahedral $CoSe_2$ nanoparticles that are well-dispersed in n-doped carbon nanotubes to facilitate increased electron transport and structural stability.[140] Anodes with novel shape-controlled and hollow $MoS_2$ nanoparticles threaded on n-doped carbon nanotubes have also been reported.[147] The abundant active sites, defects, and ion diffusion channels in the expanded $MoS_2$ layers of these hybrid anode materials facilitate enhanced potassium storage. In another modification, rose-shaped $MoS_2$ nanoparticles on reduced graphene oxide (rGO), synthesized *via* a facile hydrothermal route, have shown significantly improved cycling and capacity retention at high rates due to the stability and minimized nanoparticle aggregation provided by the rGO support and the abundant ion diffusion channels within the structure.[164] It has been observed that nanoengineered $MoSe_2$ nanosheets with a flower-like morphology where some of the nanosheets are attached to n-doped carbon layers exhibit a more stable capacity during cycling.[148] Layered $Sb_2S_3$ nanosheets are also promising as PIB anode materials in terms of enhanced cycling performance and reversible capacity due to the soft layered structure of these

Open Access Article. Published on 24 Nyenyenyani 2023. Downloaded on 2024-08-06 15:29:40.
This article is licensed under a Creative Commons Attribution-NonCommercial 3.0 Unported Licence.

materials.[143] Hybrid PIB anode nanostructures synthesized with $V_5S_8$ nanosheets supported on novel hollow carbon nanospheres have shown the most efficient rate capability among the metal chalcogenide-based anode materials synthesized so far.[150,165,166]

In summary, PIBs have the potential to achieve higher working voltages than Li and Na-ion batteries. They consist of earth-abundant source materials and facilitate an increased diffusion rate and ion conductivity compared to SIBs. These attributes make PIBs attractive for electrochemical energy storage. Two-dimensional metal chalcogenides (*e.g.*, $MoS_2$, $VS_2$, $Sb_2S_3$, $SnS_2$, $FeS_2$, ZnS, and $V_5S_8$) have been explored as promising next-generation anode materials for PIBs in both conversion and conversion/alloying types of anodes. One limitation of chalcogenide-based anodes is the formation of potassium polychalcogenide residues during the deep potassiation phase that hinder the transport of K-ions. Therefore, novel approaches like controlling the discharge depth during the K-ion intercalation, using hybrid and nanoscale chalcogenides as anode materials, ternary alloying *via* adding another cation or anion within the chalcogenide anode material, and adding a nanoscale carbonaceous support have been effectively applied in recent years to further enhance the rate capability and long-term cycling stability of PIBs.

## 5. Flexible supercapacitors

Wearable and portable electronics such as mobile phones, health-tracking devices, and laptops have become an inherent part of modern life and have revolutionized our living conditions. Flexible energy storage devices like flexible supercapacitors are the key to sustaining these next-generation

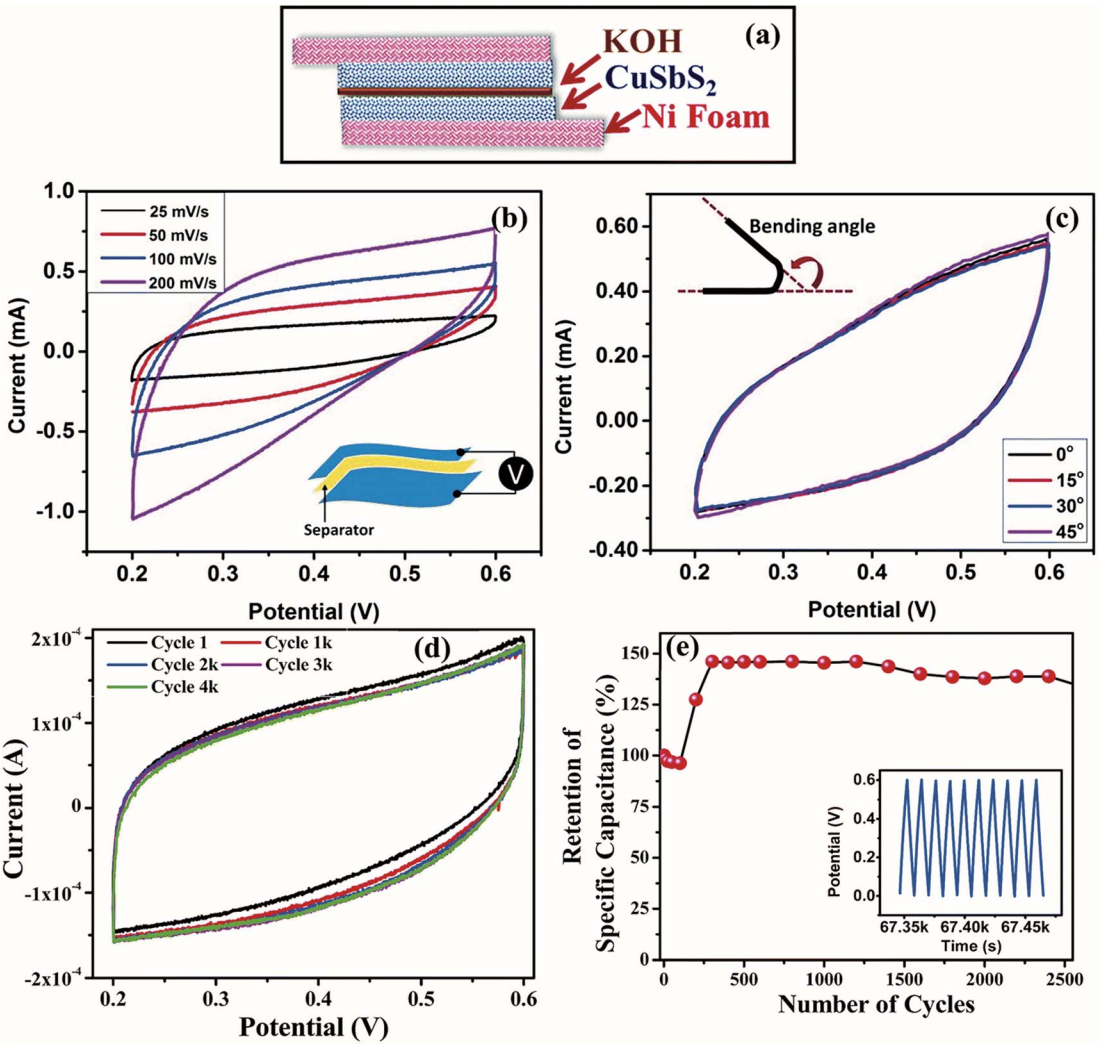


Fig. 5 Flexible supercapacitor assembly based on $CuSbS_2$ nanoplates. (a) Schematic of a flexible quasi-solid-state supercapacitor device fabricated using 55 ± 6.5 nm $CuSbS_2$ nanoplates, (b) cyclic voltammogram curves of the $CuSbS_2$ nanoplate supercapacitor device at different scan rates using KOH, (c) cyclic voltammogram curves of the $CuSbS_2$ nanoplate supercapacitor device at different bending angles, (d) cyclic voltammogram curves showing cyclic stability of the $CuSbS_2$ nanoplate device, and (e) cycling performance of the $CuSbS_2$ nanoplate supercapacitor device at a constant current of 1 mA. The inset shows the first few cycles of the charge–discharge curves. Reproduced with permission from Ramasamy *et al.*, *J. Mater. Chem. A*, 2015, **3**, 13263.[171]


© 2023 The Author(s). Published by the Royal Society of Chemistry

Open Access Article. Published on 24 Nyenyenyani 2023. Downloaded on 2024-08-06 15:29:40.
This article is licensed under a Creative Commons Attribution-NonCommercial 3.0 Unported Licence.

compact and wearable technologies. They combine the high-power density, rapid charging/discharging capability, and longer lifetime with mechanical flexibility. Each component of a flexible supercapacitor from the case to the electrode is flexible, providing a suitable platform for modern portable electronics.[7,167,168] A flexible electrode material greatly influences the overall performance, structural flexibility, and stability and is therefore one of the major components of a supercapacitor. Traditional carbonaceous materials cannot meet the high energy density required for commercial viability of these next-generation electrochemical energy storage devices. On the other hand, transition-metal chalcogenides with their high specific capacitance, excellent storage capacity and electron/ion diffusion, long operation lifetime, and morphology-tunable synthesis strategies are attractive candidates as electrode materials for flexible supercapacitors (Fig. 5). Chalcogenide-based materials can be engineered to have excellent mechanical properties required for high-quality flexible supercapacitors. The morphology of the electrode materials also plays a major role in realizing high-performance flexible supercapacitors, and as a result hollow and linear shapes of the transition-metal chalcogenides have been investigated. One example is a novel nanowire array of $Ni_3Co_6S_8$ chalcogenides on nitrogen-doped flexible carbon foam prepared *via* a facile hydrothermal approach.[169] The unique morphology of the chalcogenide electrode facilitates enhanced electrochemical performance in terms of specific capacity (243 mA h $g^{-1}$), rate capability, as well as cycling stability (*i.e.*, 84% specific capacitance after 10 000 cycles) due to the increased efficiency of consumption of the active material. Zhai *et al.* developed a new chalcogenide-based electrode material combining two transition metal sulfides (*i.e.*, copper sulfide and zinc sulfide) having high pseudo-capacitance with a porous carbon substrate having excellent double-layer capacitance.[170] The electrode induced a transformative increase in the energy density of the flexible supercapacitor, which is important for commercial viability and large-scale applicability of the technology. Layered chalcogenides are another class of promising electrode materials for flexible supercapacitors.[28,171–174] The limited conductivity in these layered materials has been addressed *via* various novel strategies. For example, InSe-based electrodes have been incorporated into an interdigitated and flexible micro supercapacitor technology to bring a breakthrough enhancement in the mobility of charge carriers. The structure of these thin layered chalcogenide materials also greatly influences their inherent properties and can therefore be used to tune the electrical conductivity of these materials.[173] Hu *et al.* added hydrogen to $Cu_2WS_4$ layered nanosheets and the resulting materials transitioned from semiconductor into metallic, which induced a huge increase in the electrical conductivity.[174] In another novel electrode material, ultrathin two-dimensional structures of $Ti_3C_2T_x$ MXene embedded with $FeCo_2S_4$ chalcogenide nanoparticles have been deposited *in situ* on polyacrylonitrile/polyvinylpyrrolidone-modified carbon nanofibers *via* electrospinning.[175] This flexible device facilitates rapid and continuous transport of electrolyte and provides breakthrough cycling stability and improved sulfide conductivity. Recent studies have also highlighted the remarkable potential of layered $MoS_2$ and $MoSe_2$ chalcogenides for flexible supercapacitor electrodes.[176] For example, a detailed investigation of the intercalation properties of $MoS_2$ has revealed its excellent specific capacitance and energy density in both aqueous and organic phases.[177] $MoS_2$ synthesized on carbon nanofibers *via* a microwave-assisted hydrothermal approach has also showed remarkable electrochemical performance.[178] Therefore, transition-metal chalcogenides have emerged as attractive components of electrodes that can meet the high energy density and specific capacitance required for next-generation flexible supercapacitors.

Therefore, the transition-metal chalcogenides have emerged as attractive electrode materials for high-performance flexible supercapacitors due to their inherently high specific capacitance and storage capacity coupled with their tunable mechanical properties. The electrochemical properties of the chalcogenides including rate, cycling stability, and specific capacity can be further enhanced through shape-control while the mechanical properties are further improved using flexible carbon-based supports. One such example of an improved electrode material for flexible supercapacitors is the $Ni_3Co_6S_8$ nanowire array supported on nitrogen-doped carbon foams. Layered chalcogenides are also attractive for flexible supercapacitors as the interlayer spacing can be controlled to achieve enhanced electrical conductivity in these materials. For example, $MoS_2$ nanoparticles supported on carbon nanofibers exhibit remarkable electrochemical performance as flexible supercapacitors. A vast increase in cycling stability has also been achieved with hybrid materials containing chalcogenide nanoparticles embedded in MXenes.

## 6. Future perspectives

Transition-metal chalcogenides and their layered architectures offer a unique class of materials with tunable properties for next-generation electrochemical energy storage devices. For example, our group has realized layered $CuSbS_2$ nanoplates with tunable thickness ranging from six to several layers and $CuSbS_2$ mesobelts that can be exfoliated to a monolayer thickness. These materials offer thickness-dependent electronic and optical properties and are attractive as electrodes for next-generation flexible supercapacitors.[28,171,179] Our group has also synthesized a new class of multinary $Cu_2ZnAS_{4-x}$ and $CuZn_2AS_4$ (A = Al, Ga, In) nanocrystals in the metastable wurtzite phase. The electronic structures of these new chalcogenide semiconductors show a dependence on the ionic radius of the group III cation, which can be tuned to achieve a desired electronic property for electrochemical energy storage. However, the practical viability of transition-metal chalcogenides as standalone electrode materials for batteries and flexible supercapacitors is limited due to their inherent constraints in structural stability and charge transport. Therefore, several novel strategies have been realized to further enhance the electrochemical and structural properties of the chalcogenides. Among them, various organic and inorganic materials for support, hybrid nanostructures with carbonaceous or

Open Access Article. Published on 24 Nyenyenyani 2023. Downloaded on 2024-08-06 15:29:40.
This article is licensed under a Creative Commons Attribution-NonCommercial 3.0 Unported Licence.

conducting polymeric materials, doping with heteroatoms, and realizing multinary chalcogenide compositions have paved the way for attractive electrochemical properties and viability of chalcogenide-based electrodes for energy storage. A three-dimensional porous network provides a key material platform for various chalcogenide-based electrodes for electrochemical energy storage, but limited information is currently available on their charge transport dynamics. Understanding the mechanisms of ion/electron diffusion in these new hybrid porous nanostructures through advanced material characterization tools including high-throughput synchrotron X-ray diffraction, small-angle X-ray scattering, and electron energy loss spectroscopy will be the key to realizing practically viable and high-energy density electrodes required for emerging energy storage technologies.[180]

Tellurides have higher volumetric energy density and unique electronic conductivity as compared to sulfides and selenides, offering an attractive alternative for high-throughput electrochemical energy storage in terms of facilitating lightweight and miniaturized next-generation devices.[181] The larger size of the Te ion favors enhanced rates of electrochemical energy conversion reaction. The larger interlayer spacing in tellurides provides a platform for increased diffusion of ions. Tellurides in the nanoscale form also offer higher structural stability to withstand volume expansion during the electrochemical energy conversion process. Therefore, these materials could be the key to portable and enhanced energy storage.

Electrosorption in the new layered and porous electrode materials that have been realized for high-throughput energy storage applications involves complex capacitive mechanisms beyond the traditional non-faradaic electric double-layer capacitance and faradaic charge transfer *via* pseudocapacitance. The unique electrolyte confinement in these materials involves new phenomena at the interface of the electric double layer and pseudocapacitive charge transfer, which open the scope for rich innovations in future energy storage technologies.[182]

One of the niche future directions for electrochemical energy storage is realizing hybrid devices that synergize multiple desirable properties such as high energy and power densities, long cycle-life, and rapid self-charging within a single device. For example, an asymmetric supercapacitor combines a battery-type electrode with a supercapacitor electrode to exploit the different potential windows of the electrodes for achieving a four-fold higher energy density as compared to regular supercapacitors.[183–190] However, the specific power and cycling life can be limiting metrics for these hybrid platforms. Therefore, different battery technologies and supercapacitors have been hybridized to achieve an alternative class of energy storage devices that can meet both the high energy and high power density requirements.[191–193] With the increasing application of portable and wearable electronics, next-generation energy storage devices in the form of self-charging supercapacitors have been developed that integrates energy harvesting from sustainable sources (*e.g.*, wind, water, and solar) and supercapacitor technologies within the same device.[194–196] These hybrid technologies synergize energy harvesting from renewable sources with the advantages of supercapacitors to achieve the next frontier of electrochemical energy storage devices.

## Conflicts of interest

There are no conflicts to declare.

## Acknowledgements

SP acknowledges the AFRL/DAGSI Ohio-Student Faculty fellowship RX-2210, University of Dayton's (UD) Research Council Summer grant, and UD Chemical and Materials Engineering for support. SP and AG acknowledge ORNL NTI and ORNL STEM, respectively, as this research was conducted as part of a user project at the Center for Nanophase Materials Sciences (CNMS), which is a US Department of Energy, Office of Science User Facility at Oak Ridge National Laboratory.

## References

1 A. Bielecki, S. Ernst, W. Skrodzka and I. Wojnicki, *Environ. Sci. Pollut. Res.*, 2020, **27**, 11506.
2 K. Mehta, M. Ehrenwirth, C. Trinkl, W. Zorner and R. Greenough, *Energies*, 2021, **14**, 2805.
3 R. Marks-Bielska, S. Bielski, K. Pik and K. Kurowska, *Energies*, 2020, **13**, 4624.
4 K. Lukasiewicz, P. Pietrzak, J. Kraciuk, E. Kacperska and M. Cieciora, *Energies*, 2022, **15**, 8284.
5 K. Mensah-Darkwa, D. N. Ampong, E. Agyekum, F. M. de Souza and R. K. Gupta, *Energies*, 2022, **15**, 4052.
6 M. Dai and R. Wang, *Small*, 2021, **17**, 2006813.
7 S. Palchoudhury, K. Ramasamy, R. K. Gupta and A. Gupta, *Front. Mater.*, 2019, **5**, 83.
8 P. Galek, A. Mackowiak, P. Bujewska and K. Fic, *Front. Energy Res.*, 2020, **8**, 139.
9 P. Simon and Y. Gogotsi, *Nat. Mater.*, 2008, **7**, 845.
10 H. Budde-Meiwes, J. Drillkens, B. Lunz, J. Muennix, S. Rothgang, J. Kowal and D. U. A. Sauer, *Proc. Inst. Mech. Eng., Part D*, 2013, **227**, 761.
11 J. Theerthagiri, K. Karuppasamy, G. Durai, A. S. Rana, P. Arunachalam, K. Sangeetha, P. Kuppusami and H. S. Kim, *Nanomater*, 2018, **8**, 256.
12 G. A. Muller, J. B. Cook, H. S. Kim, S. H. Tolbert and B. Dunn, *Nano Lett.*, 2015, **15**, 1911.
13 Y. Zhang, L. Zhang, T. A. Lv, P. K. Chu and K. F. Huo, *ChemSusChem*, 2020, **13**, 1114.
14 T. Lv, G. Zhu, S. Dong, Q. Kong, Y. Peng, S. Jiang, G. Zhang, Z. Yang, S. Yang, X. Dong, H. Pang and Y. Zhang, *Angew. Chem., Int. Ed.*, 2022, **62**, e202216089.
15 M. F. Sajjad, F. Cheng and W. Lu, *RSC Adv.*, 2021, **11**, 25450.
16 J. Cherusseri, N. Choudhary, K. S. Kumar, Y. Jung and J. Thomas, *Nanoscale Horiz.*, 2019, **4**, 840.
17 M. A. Bissett, S. D. Worrall, I. A. Kinloch and R. A. W. Dryfe, *Electrochim. Acta*, 2016, **201**, 30.
18 H. Xia, Q. Xu and J. Zhang, *Nano-Micro Lett.*, 2018, **10**, 66.


© 2023 The Author(s). Published by the Royal Society of Chemistry

Open Access Article. Published on 24 Nyenyenyani 2023. Downloaded on 2024-08-06 15:29:40.
This article is licensed under a Creative Commons Attribution-NonCommercial 3.0 Unported Licence.

19 S. Song, Y. Sim, S. Kim, J. Hwa, I. Oh, W. Na, D. Lee, J. Wang, S. Yan, Y. Liu, J. Kwak, J. Chen, H. Cheong, J. Yoo, Z. Lee and S. Kwon, *Nat. Electron.*, 2020, **3**, 207.
20 Y. Sun, Y. Wang, J. Chen, K. Fujisawa, C. Holder, J. Miller, V. Crespi, M. Terrones and R. Schaak, *Nat. Chem.*, 2020, **12**, 284.
21 J. Fenton, B. Steimle and R. Schaak, *Science*, 2018, **360**, 513.
22 H. Lim, Y. Nakanishi, Z. Liu, J. Pu, M. Maruyama, T. Endo, C. Ando, H. Shimizu, K. Yanagi, S. Okada, T. Takenobu and Y. Miyata, *Nano Lett.*, 2021, **21**, 243.
23 W. Li, X. Wei, H. Dong, Y. Ou, S. Xiao, Y. Yang, P. Xiao and Y. Zhang, *Front. Chem.*, 2020, **8**, 189.
24 S. Palchoudhury, K. Ramasamy and A. Gupta, *Nanoscale Adv.*, 2020, **2**, 3069.
25 A. Ghosh, S. Palchoudhury, T. Rajalingam, Z. Zhou, N. Naghibolashrafi, K. Ramasamy and A. Gupta, *Chem. Commun.*, 2016, **52**, 264.
26 N. Tapia-Ruiz, A. Armstrong, H. Alptekin, M. Amores, H. Au, J. Barker, R. Boston, W. Brant, J. Brittain, Y. Y. Chen, *et al.*, *J. Phys.: Energy*, 2021, **3**, 031503.
27 Q. Pang, J. Meng, S. Gupta, X. Hong, C. Kwok, J. Zhao, Y. Jin, L. Xu, O. Karahan, Z. Wang, S. Toll, L. Mai, L. Nazar, M. Balasubramanium, B. Narayan and D. R. Sadoway, *Nature*, 2022, **608**, 704.
28 K. Ramasamy, R. K. Gupta, S. Palchoudhury, S. Ivanov and A. Gupta, *Chem. Mater.*, 2015, **27**, 379.
29 J. Goodenough and K. Park, *J. Am. Chem. Soc.*, 2013, **135**, 1167.
30 K. Turcheniuk, D. Bondarev, V. Singhal and G. Yushin, *Nature*, 2018, **559**, 467.
31 J. Xie and Y. Lu, *Nat. Commun.*, 2020, **11**, 2499.
32 Y. Sun, N. Liu and Y. Cui, *Nat. Energy*, 2016, **1**, 16071.
33 X. Chen, J. Zhou, J. Li, H. Luo, L. Mei, T. Wang, J. Zhu and Y. Zhang, *RSC Adv.*, 2019, **9**, 35045.
34 R. Jin, W. Cui and R. Li, *Solid State Ionics*, 2021, **366**, 115660.
35 Q. Wang, K. Kalantar-Zadeh, A. Kis, J. Coleman and M. Strano, *Nat. Nanotechnol.*, 2012, **7**, 699.
36 P. Zhou, G. Collins, Z. Hens, K. Ryan, H. Geaney and S. Singh, *Nanoscale*, 2020, **12**, 22307.
37 L. Peng, Y. Zhu, D. Chen, R. Ruoff and G. Yu, *Adv. Energy Mater.*, 2016, **6**, 1600025.
38 B. Zhang, X. Ji, K. Xu, C. Chen, X. Xiong, J. Xiong, Y. Yao, L. Miao and J. Jiang, *Electrochim. Acta*, 2016, **217**, 1–8.
39 C. Wei, Z. Hou, H. Sun and J. Wang, *Front. Chem.*, 2021, **9**, 802788.
40 L. Chen, H. Jiang, H. Jiang, H. Zhang, S. Guo, Y. Hu and C. Li, *Adv. Energy Mater.*, 2017, **7**, 1602782.
41 H. Xu, L. Sun, W. Li, M. Gao, Q. Zhou, P. Li, S. Yang and J. Lin, *Chem. Eng. J.*, 2022, **435**(PT 2), 135129.
42 X. Li, J. Fu, Y. Sun, M. Sun, S. Cheng, K. Chen, X. Yang, Q. Lou, T. Xu, Y. Shang, J. Xu, Q. Chen and C. Shan, *Nanoscale*, 2019, **11**, 13343.
43 F. Ming, H. Liang, Y. Lei, W. Zhang and H. Alshareef, *Nano Energy*, 2018, **53**, 11–16.
44 Y. Wang, D. Kong, W. Shi, B. Liu, G. Sim, Q. Ge and H. Yang, *Adv. Energy Mater.*, 2016, **6**, 1601057.
45 C. Chen, X. Xie, B. Anasori, A. Sarycheva, T. Makaryan, M. Zhao, P. Urbankowski, L. Miao, J. Jiang and Y. Gogotsi, *Angew. Chem., Int. Ed.*, 2018, **57**, 1846.
46 M. Cao, L. Gao, X. Lv and Y. Shen, *J. Power Sources*, 2017, **350**, 87.
47 P. Geng, L. Wang, M. Du, Y. Bai, W. Li, Y. Liu, S. Chen, P. Braunstein, Q. Xu and H. Pang, *Adv. Mater.*, 2022, **34**, 2107836.
48 S. Zheng, Y. Sun, H. Xue, P. Braunstein, W. Huang and H. Pang, *Natl. Sci. Rev.*, 2022, **9**, nwab197.
49 Y. Ding, C. Wang, R. Zheng, S. Maitra, G. Zhang, T. Barakat, S. Roy, B. Su and L. Chen, *EnergyChem*, 2022, **4**, 100081.
50 L. Guo, Z. Mu, P. Da, Z. Weng, P. Xi and C. Yan, Hollow structures with rare earths: Synthesis and electrocatalytic applications, *EnergyChem*, 2022, **4**, 100088.
51 J. Broadhead, F. A. Trumbore and S. Basu, *J. Electroanal. Chem.*, 1981, **118**, 241.
52 L. Li, Z. Li, A. Yoshimura, C. Sun, T. Wang, Y. Chen, Z. Chen, A. Littlejohn, Y. Xiang, P. Hundekar, S. Bartolucci, J. Shi, S. Shi, V. Meunier, G. Wang and N. Koratkar, *Nat. Commun.*, 2019, **10**, 1764.
53 J. Zhao, R. Huang, P. Ramos, Y. Yue, Q. Wu, M. Pavanello, J. Zhou, X. Kuai, L. Gao, H. He and Y. Wang, *ACS Appl. Mater. Interfaces*, 2017, **9**, 31181.
54 W. Fang, H. Zhao, Y. Xie, J. Fang, J. Xu and Z. Chen, *ACS Appl. Mater. Interfaces*, 2015, **7**, 13044.
55 H. Hwang, H. Kim and J. Cho, *Nano Lett.*, 2011, **11**, 4826.
56 Y. Chen, B. Song, X. Tang, L. Lu and J. Xue, *Small*, 2014, **10**, 1536.
57 D. Chen, G. Ji, B. Ding, Y. Ma, B. Qu, W. Chen and J. Lee, *Nanoscale*, 2013, **5**, 7890.
58 Y. Shi, Y. Wang, J. Wong, A. Tan, C. Hsu, L. Li, Y. Lu and H. Yang, *Sci. Rep.*, 2013, **3**, 2169.
59 C. Hu, L. Lv, J. Xue, M. Ye, L. Wang and L. Qu, *Chem. Mater.*, 2015, **27**, 5253.
60 Z. Wu, W. Ren, L. Xu, F. Li and H. Cheng, *ACS Nano*, 2011, **5**, 5463.
61 P. Xiong, B. Liu, V. Teran, Y. Zhao, L. Peng, X. Wang and G. Yu, *ACS Nano*, 2014, **8**, 8610.
62 X. Huang, X. Xia, Y. Yuan and F. Zhou, *Electrochim. Acta*, 2011, **56**, 4960.
63 W. Li, F. Wang, S. Feng, J. Wang, Z. Sun, B. Li, Y. Li, J. Yang, A. Elzatahry, Y. Xia and D. Zhao, *J. Am. Chem. Soc.*, 2013, **135**, 18300.
64 S. Chen, Y. Xin, Y. Zhou, Y. Ma, H. Zhou and L. Qi, *Energy Environ. Sci.*, 2014, **7**, 1924.
65 Y. Zhao, L. Peng, B. Liu and G. Yu, *Nano Lett.*, 2014, **14**, 2849.
66 X. Rui, X. Zhao, Z. Lu, H. Tan, D. Sim, H. Hng, R. Yazami, T. Lim and Q. Yan, *ACS Nano*, 2013, **7**, 5637.
67 M. Naguib, M. Kurtoglu, V. Presser, J. Lu, J. Niu, M. Heon, L. Hultman, Y. Gogotsi and M. Barsoum, *Adv. Mater.*, 2011, **23**, 4248.
68 M. Naguib, J. Halim, J. Lu, K. Cook, L. Hultman, Y. Gogotsi and M. Barsoum, *J. Am. Chem. Soc.*, 2013, **135**, 15966.
69 G. Che, K. Jirage, E. Fisher, C. Martin and H. Yoneyama, *J. Electrochem. Soc.*, 1997, **144**, 4296.

Open Access Article. Published on 24 Nyenyenyani 2023. Downloaded on 2024-08-06 15:29:40.
This article is licensed under a Creative Commons Attribution-NonCommercial 3.0 Unported Licence.

70 J. Cho, Y. Kim, B. Kim, J. Lee and B. Park, *Angew. Chem., Int. Ed.*, 2003, **42**, 1618.
71 F. Lin, I. Markus, D. Nordlund, T. Weng, M. Asta, H. Xin and M. Doeff, *Nat. Commun.*, 2014, **5**, 3529.
72 C. Gong, Z. Xue, S. Wen, Y. Ye and X. Xie, *J. Power Sources*, 2016, **318**, 93.
73 M. Lee, S. Lee, P. Oh, Y. Kim and J. Cho, *Nano Lett.*, 2014, **14**, 993.
74 A. Yamada, S. Chung and K. Hinokuma, *J. Electrochem. Soc.*, 2001, **148**, A224.
75 N. Nitta, F. Wu, J. Lee and G. Yushin, *Mater. Today*, 2015, **18**, 252.
76 M. Fichtner, K. Edstrom, E. Ayerbe, M. Berecibar, A. Bhowmik, I. Castelli, S. Clark, R. Dominko, M. Erakca, A. Franco, A. Grimaud, B. Horstmann, A. Latz, H. Lorrman, M. Meeus, R. Narayan, F. Pammer, J. Ruhland, H. Stein, T. Vegge and M. Weil, *Adv. Energy Mater.*, 2022, **12**, 2102904.
77 Z. Ali, T. Zhang, M. Asif, L. Zhao, Y. Yu and Y. Hou, *Mater. Today*, 2020, **35**, 131.
78 Y. Fang, D. Luan, Y. Chen, S. Gao and X. Lou, *Angew. Chem., Int. Ed.*, 2020, **59**, 2644.
79 G. Eshetu, G. Elia, M. Armand, M. Forsyth, S. Komaba, T. Rojo and S. Passerini, *Adv. Energy Mater.*, 2020, **10**, 2000093.
80 J. Ma, Y. Li, N. S. Grundish, J. B. Goodenough, Y. Chen, L. Guo, Z. Peng, X. Qi, F. Yang, L. Qie, C. Wang, B. Huang, Z. Huang, L. Chen, D. Su, G. Wang, X. Peng, Z. Chen, J. Yang, S. He, X. Zhang, H. Yu, C. Fu, M. Jiang, W. Deng, C. Sun, Q. Pan, Y. Tang, X. Li, X. Ji, F. Wan, Z. Niu, F. Lian, C. Wang, G. G. Wallace, M. Fan, Q. Meng, S. Xin, Y. Guo and L. Wan, The 2021 battery technology roadmap, *J. Phys. D: Appl. Phys.*, 2021, **54**, 183001.
81 S. Li, S. Luo, L. Rong, L. Wang, Z. Xi, Y. Liu, Y. Zhou, Z. Wan and X. Kong, *Molecules*, 2022, **27**, 3989.
82 S. Dai, L. Wang, M. Cao, Z. Zhong, Y. Shen and M. Wang, *Mater. Today Energy*, 2019, **12**, 114.
83 Y. Fang, X. Yu and X. Lou, *Angew. Chem., Int. Ed.*, 2019, **58**, 7744.
84 Z. Li, Y. Fang, J. Zhang and X. Lou, *Adv. Mater.*, 2018, **30**, 1800525.
85 E. Yang, H. Ji and Y. Jung, *J. Phys. Chem. C*, 2015, **119**, 26374.
86 Y. Fang, X. Yu and X. Lou, *Adv. Mater.*, 2018, **30**, 1706668.
87 Y. Huang, M. Xie, Z. Wang, Y. Jiang, G. Xiao, S. Li, L. Li, F. Wu and R. Chen, *Energy Storage Mater.*, 2018, **11**, 100.
88 K. Zhang, M. Park, L. Zhou, G. Lee, J. Shin, Z. Hu, S. Chou, J. Chen and Y. Kang, *Angew. Chem., Int. Ed.*, 2016, **55**, 12822.
89 Z. Li, W. Feng, Y. Lin, X. Liu and H. Fei, *RSC Adv.*, 2016, **6**, 70632.
90 S. Chen, S. Huang, Y. Zhang, S. Fan, D. Yan, Y. Shang, M. Pam, Q. Ge, Y. Shi and H. Yang, *Nano Energy*, 2020, **69**, 104389.
91 J. Zhou, L. Wang, M. Yang, J. Wu, F. Chen, W. Huang, N. Han, H. Ye, F. Zhao, Y. Li and Y. Li, *Adv. Mater.*, 2017, **29**, 1702061.
92 D. Yu, Q. Pang, Y. Gao, Y. Wei, C. Wang, G. Chen and F. Du, *Energy Storage Mater.*, 2018, **11**, 1–7.
93 Y. Pang, S. Zhang, L. Liu, J. Liang, Z. Sun, Y. Wang, C. Xiao, D. Ding and S. Ding, *J. Mater. Chem. A*, 2017, **5**, 17963.
94 D. Xie, X. Xia, Y. Zhong, Y. Wang, D. Wang, X. Wang and J. Tu, *Adv. Energy Mater.*, 2021, **11**, 2003595.
95 N. Mahmood, T. Tang and Y. Hou, *Adv. Energy Mater.*, 2016, **6**, 1600374.
96 D. Sun, D. Ye, P. Liu, Y. Tang, J. Guo, L. Wang and H. Wang, *Adv. Energy Mater.*, 2018, **8**, 1702383.
97 X. Hu, Y. Li, G. Zeng, J. Jia, H. Zhan and Z. Wen, *ACS Nano*, 2018, **12**, 1592.
98 X. Xie, T. Makaryan, M. Zhao, K. Van Aken, Y. Gogotsi and G. Wang, *Adv. Energy Mater.*, 2016, **6**, 1502161.
99 X. Xiong, C. Yang, G. Wang, Y. Lin, X. Ou, J. Wang, B. Zhao, M. Liu, Z. Lin and K. Huang, *Energy Environ. Sci.*, 2017, **10**, 1757.
100 B. Qu, C. Ma, G. Ji, C. Xu, J. Xu, Y. Meng, T. Wang and J. Lee, *Adv. Mater.*, 2014, **26**, 3854.
101 Y. Liu, Y. Yang, X. Wang, Y. Dong, Y. Tang, Z. Yu, Z. Zhao and J. Qiu, *ACS Appl. Mater. Interfaces*, 2017, **9**, 15484.
102 Z. Wei, L. Wang, M. Zhuo, W. Ni, H. Wang and J. Ma, *J. Mater. Chem. A*, 2018, **6**, 12185.
103 R. Chen, S. Li, J. Liu, Y. Li, F. Ma, J. Liang, X. Chen, Z. Miao, J. Han, T. Wang and Q. Li, *Electrochim. Acta*, 2018, **282**, 973.
104 X. Yang, R. Zhang, N. Chen, X. Meng, P. Yang, C. Wang, Y. Zhang, Y. Wei, G. Chen and F. Du, *Chem.–Eur. J.*, 2016, **22**, 1445.
105 Y. Dong, W. Shi, P. Lu, J. Qin, S. Zheng, B. Zhang, X. Bao and Z. Wu, *J. Mater. Chem. A*, 2018, **6**, 14324.
106 L. Zhou, K. Zhang, J. Sheng, Q. An, Z. Tao, Y. Kang, J. Chen and L. Mai, *Nano Energy*, 2017, **35**, 281.
107 Z. Shadike, M. Cao, F. Ding, L. Sang and Z. Fu, *Chem. Commun.*, 2015, **51**, 10486.
108 J. Deng, Q. Gong, H. Ye, K. Feng, J. Zhou, C. Zha, J. Wu, J. Chen, J. Zhong and Y. Li, *ACS Nano*, 2018, **12**, 1829.
109 J. Li, J. Li, D. Yan, S. Hou, X. Xu, T. Lu, Y. Yao, W. Mai and L. Pan, *J. Mater. Chem. A*, 2018, **6**, 6595.
110 D. Zhang, W. Sun, Y. Zhang, Y. Dou, Y. Jiang and S. Dou, *Adv. Funct. Mater.*, 2016, **26**, 7479.
111 C. Dong, J. Liang, Y. He, C. Li, X. Chen, L. Guo, F. Tian, Y. Qian and L. Xu, *ACS Nano*, 2018, **12**, 8277.
112 B. Dong, W. Li, X. Huang, Z. Ali, T. Zhang, Z. Yang and Y. Hou, *Nano Energy*, 2019, **55**, 37.
113 D. Su, S. Dou and G. Wang, *Chem. Commun.*, 2014, **50**, 4192.
114 Y. Wang, D. Kong, S. Huang, Y. Shi, M. Ding, Y. Lim, T. Xu, F. Chen, X. Li and H. Yang, *J. Mater. Chem. A*, 2018, **6**, 10813.
115 Y. Liu, N. Zhang, H. Kang, M. Shang, L. Jiao and J. Chen, *Chem.–Eur. J.*, 2015, **21**, 11878.
116 Z. Liang, H. Tu, K. Zhang, Z. Kong, M. Huang, D. Xu, S. Liu, Y. Wu and X. Hao, *Chem. Eng. J.*, 2022, **437**, 135421.
117 Y. Chen, H. Liu, X. Guo, S. Zhu, Y. Zhao, S. Iikubo and T. Ma, *ACS Appl. Mater. Interfaces*, 2021, **13**, 39248.
118 X. Yu and X. Lou, *Adv. Energy Mater.*, 2018, **8**, 1701592.
119 L. Shen, L. Yu, H. Wu, X. Yu, X. Zhang and X. Lou, *Nat. Commun.*, 2015, **6**, 6694.


© 2023 The Author(s). Published by the Royal Society of Chemistry

Open Access Article. Published on 24 Nyenyenyani 2023. Downloaded on 2024-08-06 15:29:40.
This article is licensed under a Creative Commons Attribution-NonCommercial 3.0 Unported Licence.

120 J. Li, B. Liu, M. Li, Q. Zhou, Q. Chen, C. Guo and L. Zhang, *Eur. J. Inorg. Chem.*, 2018, **2018**, 3036.
121 H. Geng, J. Yang, Z. Dai, Y. Zhang, Y. Zheng, H. Yu, H. Wang, Z. Luo, Y. Guo, H. Fan, X. Wu, J. Zheng, Y. Yang, Q. Yan and H. Gu, *Small*, 2017, **13**, 1603490.
122 S. Dong, C. Li, X. Ge, Z. Li, X. Miao and L. Yin, *ACS Nano*, 2017, **11**, 6474.
123 X. Liu, Y. Wang, Z. Wang, T. Zhou, M. Yu, L. Xiu and J. Qiu, *J. Mater. Chem. A*, 2017, **5**, 10398.
124 H. Dai, W. Xu, Z. Hu, Y. Chen, X. Wei, B. Yang, Z. Chen, J. Gu, D. Yang, F. Xie, W. Zhang, R. Guo, G. Zhang and W. Wei, *Front. Energy Res.*, 2020, **8**, 97.
125 N. Tanibata, K. Noi, A. Hayashi and M. Tatsumisago, *RSC Adv.*, 2014, **4**, 17120.
126 T. Krauskopf, S. P. Culver and W. G. Zeier, *Inorg. Chem.*, 2018, **57**, 4739.
127 S. Takeuchi, K. Suzuki, M. Hirayama and R. Kanno, *J. Solid State Chem.*, 2018, **265**, 353.
128 Q. Zhang, C. Zhang, Z. Hood, M. Chi, C. Liang, N. H. Jalarvo, M. Yu and H. Wang, *Chem. Mater.*, 2020, **32**, 2264.
129 S. Bo, Y. Wang, J. Kim, W. Richards and G. Ceder, *Chem. Mater.*, 2016, **28**, 252.
130 M. M. A. Mahmoud, D. P. Joubert and M. P. Molepo, *Eur. Phys. J. B*, 2019, **92**, 214.
131 Y. Wang, W. Richards, S. Bo, L. Miara and G. Ceder, *Chem. Mater.*, 2017, **29**, 7475.
132 B. Ma, Q. Jiao, Y. Zhang, X. Sun, G. Yin, X. Zhang, H. Ma, X. Liu and S. Dai, *Ceram. Int.*, 2020, **46**, 6544.
133 K. Park, D. Kim, H. Kwak, S. Jung, H. Lee, A. Banerjee, J. Lee and Y. Jung, *J. Mater. Chem. A*, 2018, **6**, 17192.
134 F. Tsuji, N. Tanibata, A. Sakuda, A. Hayashi and M. Tatsumisago, *Chem. Lett.*, 2018, **47**, 13.
135 Z. Zhu, I. Chu, Z. Deng and S. Ong, *Chem. Mater.*, 2015, **27**, 8318.
136 N. J. J. de Klerk and M. Wagemaker, *Chem. Mater.*, 2016, **28**, 3122.
137 H. Wan, L. Cai, W. Weng, J. Mwizerwa, J. Yang and X. Yao, *J. Power Sources*, 2020, **449**, 227515.
138 S. Yubuchi, A. Ito, N. Masuzawa, A. Sakuda, A. Hayashi and M. Tatsumisago, *J. Mater. Chem. A*, 2020, **8**, 1947.
139 J. Zhou, Y. Liu, S. Zhang, T. Zhou and Z. Guo, *InfoMat*, 2020, **2**, 437.
140 Q. Yu, B. Jiang, J. Hu, C. Lao, Y. Gao, P. Li, Z. Liu, G. Suo, D. He, W. Wang and G. Yin, *Adv. Sci.*, 2018, **5**, 1800782.
141 W. Zhang, Y. Liu and Z. Guo, *Sci. Adv.*, 2019, **5**, eaav741.
142 Y. Xu, C. Zhang, M. Zhou, Q. Fu, C. Zhao, M. Wu and Y. Lei, *Nat. Commun.*, 2018, **9**, 1720.
143 Y. Liu, Z. Tai, J. Zhang, W. Pang, Q. Zhang, H. Feng, K. Konstantinov, Z. Guo and H. Liu, *Nat. Commun.*, 2018, **9**, 3645.
144 L. Fang, J. Xu, S. Sun, B. Lin, Q. Guo, D. Luo and H. Xia, *Small*, 2019, **15**, 1804806.
145 C. He, J. Zhang, W. Zhang and T. Li, *J. Phys. Chem. C*, 2019, **123**, 5157.
146 Z. Yi, Y. Qian, J. Tian, K. Shen, N. Lin and Y. Qian, *J. Mater. Chem. A*, 2019, **7**, 12283.
147 B. Jia, Q. Yu, Y. Zhao, M. Qin, W. Wang, Z. Liu, C. Lao, Y. Liu, H. Wu, Z. Zhang and X. Qu, *Adv. Funct. Mater.*, 2018, **28**, 1803409.
148 J. Ge, L. Fan, J. Wang, Q. Zhang, Z. Liu, E. Zhang, Q. Liu, X. Yu and B. Lu, *Adv. Energy Mater.*, 2018, **8**, 1801477.
149 Y. Zhao, J. Zhu, S. Ong, Q. Yao, X. Shi, K. Hou, Z. Xu and L. Guan, *Adv. Energy Mater.*, 2018, **8**, 1802565.
150 L. Li, W. Zhang, X. Wang, S. Zhang, Y. Liu, M. Li, G. Zhu, Y. Zheng, Q. Zhang, T. Zhou, W. Pang, W. Luo, Z. Guo and J. Yang, *ACS Nano*, 2019, **13**, 7939.
151 Y. Wu, H. Huang, Y. Feng, Z. Wu and Y. Yu, *Adv. Mater.*, 2019, **31**, 1901414.
152 M. Zhang, M. Shoaib, H. Fei, T. Wang, J. Zhong, L. Fan, L. Wang, H. Luo, S. Tan, Y. Wang, J. Zhu, J. Hu and B. Lu, *Adv. Energy Mater.*, 2019, **9**, 1901663.
153 C. Chen, Y. Yang, X. Tang, R. Qiu, S. Wang, G. Cao and M. Zhang, *Small*, 2019, **15**, 1804740.
154 X. Ren, Q. Zhao, W. McCulloch and Y. Wu, *Nano Res.*, 2017, **10**, 1313.
155 H. Yu, X. Cheng, M. Xia, T. Liu, W. Ye, R. Zheng, N. Long, M. Shui and J. Shu, *Energy Storage Mater.*, 2019, **22**, 154.
156 L. Xu, P. Xiong, L. Zeng, Y. Fang, R. Liu, J. Liu, F. Luo, Q. Chen, M. Wei and Q. Qian, *Nanoscale*, 2019, **11**, 16308.
157 W. Miao, Y. Zhang, H. Li, Z. Zhang, L. Li, Z. Yu and W. Zhang, *J. Mater. Chem. A*, 2019, **7**, 5504.
158 H. He, D. Huang, Q. Gan, J. Hao, S. Liu, Z. Wu, W. Pang, B. Johannessen, Y. Tang, J. Luo, H. Wang and Z. Guo, *ACS Nano*, 2019, **13**, 11843.
159 Z. Wu, G. Liang, W. Pang, T. Zhou, Z. Cheng, W. Zhang, Y. Liu, B. Johannessen and Z. Guo, *Adv. Mater.*, 2020, **32**, 1905632.
160 H. Tian, X. Yu, H. Shao, L. Dong, Y. Chen, X. Fang, C. Wang, W. Han and G. Wang, *Adv. Energy Mater.*, 2019, **9**, 1901560.
161 F. Cheng, J. Liang, Z. Tao and J. Chen, *Adv. Mater.*, 2011, **23**, 1695.
162 X. Cao, C. Tan, M. Sindoro and H. Zhang, *Chem. Soc. Rev.*, 2018, **47**, 5997.
163 S. Mishra, *Chem. Commun.*, 2022, **58**, 10136.
164 S. Chong, L. Sun, C. Shu, S. Guo, Y. Liu, W. Wang and H. Liu, *Nano Energy*, 2019, **63**, 103868.
165 S. Liu, H. Zhang, M. Zhou, X. Chen, Y. Sun and Y. Zhang, *J. Electroanal. Chem.*, 2021, **903**, 115841.
166 C. Yang, X. Ou, X. Xiong, F. Zheng, R. Hu, Y. Chen, M. Liu and K. Huang, *Energy Environ. Sci.*, 2017, **10**, 107.
167 Q. Xue, J. Sun, Y. Huang, M. Zhu, Z. Pei, H. Li, Y. Wang, N. Li, H. Zhang and C. Zhi, *Small*, 2017, **13**, 1701827.
168 C. Zhang, X. Cai, Y. Qian, H. Jiang, L. Zhou, B. Li, L. Lai, Z. Shen and W. Huang, *Adv. Sci.*, 2018, **5**, 1700375.
169 Y. Li, J. Gong, X. Xing, J. Du, P. Xu, K. Cheng, K. Ye, K. Zhu, J. Yan, D. Cao and G. Wang, *Int. J. Energy Res.*, 2021, **45**, 5517.
170 S. Zhai, Z. Fan, K. Jin, M. Zhou, H. Zhao, Y. Zhao, F. Ge, X. Li and Z. Cai, *J. Colloid Interface Sci.*, 2020, **575**, 306.
171 K. Ramasamy, R. K. Gupta, H. Sims, S. Palchoudhury, S. Ivanov and A. Gupta, *J. Mater. Chem. A*, 2015, **3**, 13263.
172 Z. Zhai, W. Yan, L. Dong, J. Wang, C. Chen, J. Lian, X. Wang, D. Xia and J. Zhang, *Nano Energy*, 2020, **78**, 105193.

Open Access Article. Published on 24 Nyenyenyani 2023. Downloaded on 2024-08-06 15:29:40.
This article is licensed under a Creative Commons Attribution-NonCommercial 3.0 Unported Licence.

173 C. Mu, X. Sun, Y. Chang, F. Wen, A. Nie, B. Wang, J. Xiang, K. Zhai, T. Xue and Z. Liu, *J. Power Sources*, 2021, **482**, 228987.
174 X. Hu, W. Shao, X. Hang, X. Zhang, W. Zhu and Y. Xie, *Angew. Chem., Int. Ed.*, 2016, **55**, 5733.
175 S. Yan, S. Luo, Q. Wang, Y. Zhang and X. Liu, *Composites, Part B*, 2021, **224**, 109246.
176 S. Balasingam, J. Lee and Y. Jun, *Dalton Trans.*, 2015, **44**, 15491.
177 N. Feng, R. Meng, L. Zu, Y. Feng, C. Peng, J. Huang, G. Liu, B. Chen and J. Yang, *Nat. Commun.*, 2019, **10**, 1372.
178 F. Sari and J. Ting, *Sci. Rep.*, 2017, **7**, 5999.
179 K. Ramasamy, H. Sims, W. Butler and A. Gupta, *J. Am. Chem. Soc.*, 2014, **136**, 1587.
180 Y. Yang, T. Zhu, L. Shen, Y. Liu, D. Zhang, B. Zheng, J. Gong, X. Zheng and X. Gong, *SmartMat*, 2022, **3**, 349.
181 M. Han, Z. Zhou, Y. Li, Q. Chen and M. Chen, *ChemElectroChem*, 2021, **8**, 4412.
182 S. Fleischmann, Y. Zhang, X. Wang, P. Cummings, J. Wu, P. Simon, Y. Gogotsi, V. Presser and V. Augustyn, *Nat. Energy*, 2022, **7**, 222.
183 D. Gao, Z. Luo, C. Liu and S. Fan, *Green Energy Environ.*, 2022, DOI: **10.1016/j.gee.2022.02.002**.
184 F. Zhang, T. Zhang, X. Yang, L. Zhang, K. Leng, Y. Huang and Y. Chen, *Energy Environ. Sci.*, 2013, **6**, 1623.
185 V. Aravindan, J. Gnanaraj, Y. Lee and S. Madhavi, *Chem. Rev.*, 2014, **114**, 11619.
186 V. Pushparaj, M. Shaijumon, A. Kumar, S. Murugesan, L. Ci, R. Vajtai, R. Linhardt, O. Nalamasu and P. Ajayan, *Proc. Natl. Acad. Sci. U. S. A.*, 2007, **104**, 13574.
187 L. Lam and R. Louey, *J. Power Sources*, 2006, **158**, 1140.
188 M. Park, Y. Lim, J. Kim, Y. Kim, J. Cho and J. Kim, *Adv. Energy Mater.*, 2011, **1**, 1002.
189 M. Salanne, B. Rotenberg, K. Naoi, K. Kaneko, P. Taberna, C. Grey, B. Dunn and P. Simon, *Nat. Energy*, 2016, **1**, 16070.
190 F. Wang, S. Xiao, Y. Hou, C. Hu, L. Liu and Y. Wu, *RSC Adv.*, 2013, **3**, 13059.
191 D. Dubal, O. Ayyad, V. Ruiz and P. Gomez-Romero, *Chem. Soc. Rev.*, 2015, **44**, 1777.
192 L. Kouchachvili, W. Yaici and E. Entchev, *J. Power Sources*, 2018, **374**, 237.
193 B. Culpin and D. Rand, *J. Power Sources*, 1991, **36**, 415.
194 F. Fan, Z. Tian and Z. Wang, *Nano Energy*, 2012, **1**, 328.
195 Z. Wang, *ACS Nano*, 2013, **7**, 9533.
196 F. Fan, J. Luo, W. Tang, C. Li, C. Zhang, Z. Tian and Z. Wang, *J. Mater. Chem. A*, 2014, **2**, 13219.


© 2023 The Author(s). Published by the Royal Society of Chemistry